Quantification of Methane Sources in the Athabasca Oil Sands Region of Alberta by Aircraft Mass-Balance

Sabour Baray[1], Andrea Darlington[2], Mark Gordon[3], Katherine L. Hayden[2], Amy Leithead[2], Shao-Meng Li[2], Peter S.K. Liu[2], Richard L. Mittermeier[2], Samar G. Moussa[2], Jason O'Brien[2], Ralph Staebler[2], Mengistu Wolde[4], Doug Worthy[5], Robert McLaren[1]

1. Centre for Atmospheric Chemistry, York University, Toronto 2. Air Quality Research Division, Environment and Climate Change Canada, Toronto 3. Earth and Space Science and Engineering, York University, Toronto 4. National Research Council of Canada, Ottawa 5. Climate Research Division, Environment and Climate Change Canada, Toronto, Canada

Corresponding authors: Robert McLaren (rmclaren@yorku.ca) & Katherine Hayden (katherine.hayden@canada.ca)

Abstract. Aircraft-based measurements of methane (CH_4) and other air pollutants in the Athabasca Oil Sands Region (AOSR) were made during a summer intensive field campaign between August 13 and September 7 2013, in support of the Joint Canada–Alberta Implementation Plan for Oil Sands Monitoring. Chemical signatures were used to identify CH_4 sources from tailings ponds (BTEX VOC's), open-pit surface mines (NO_y and rBC) and elevated plumes from bitumen upgrading facilities (SO_2 and NO_y). Emission rates of CH_4 were determined for the five primary surface mining facilities in the region using two mass balance methods. Emission rates from source categories within each facility were estimated when plumes from the sources were spatially separable. Tailings ponds accounted for 45% of total CH_4 emissions measured from the major surface mining facilities in the region while emissions from operations in the open pit mines accounted for ~50%. The average open pit surface mining emission rates ranged from 1.2 to 2.8 tonnes of CH_4 hr^{-1} for different facilities in the AOSR. Amongst the 19 tailings ponds, Mildred Lake Settling Basin, the oldest pond in the region, was found to be responsible for the majority of tailings ponds emissions of CH_4 (>70%). The sum of measured emission rates of CH_4 from the five major facilities, 19.2 ± 1.1 tonnes CH_4 hr^{-1}, was similar to a single mass balance determination of CH_4 from all major sources in the AOSR determined from a single flight downwind of the facilities, 23.7 ± 3.7 tonnes CH_4 hr^{-1}. The measured hourly CH_4 emission rate from all facilities in the AOSR is $48 \pm 8\%$ higher than that extracted for 2013 from the Canadian Green House Gas Reporting Program, a legislated facility-reported Emissions Inventory, converted to hourly units. The measured emissions correspond to an emissions rate of 0.17 ± 0.01 Tg CH_4 yr^{-1}, if the emissions are

assumed temporally constant, an uncertain assumption. The emission rates reported here are relevant for the summer season. In future, effort should be devoted to measurements in different seasons to further our understanding of seasonal parameters impacting fugitive emissions of CH_4 and to allow better estimates of annual emissions and year to year variability.

Introduction

Methane (CH_4) is a significant greenhouse gas (GHG), second in rank to carbon dioxide (CO_2) in terms of its direct radiative forcing (Montzka et al., 2011;IPCC, 2013). Controlling emissions of CH_4 is an attractive climate control strategy because of its shorter atmospheric lifetime ($\tau \sim 9$ years) and larger global warming potential (GWP) compared to CO_2 (IPCC, 2013). Emissions of CH_4 include biogenic (animal husbandry, landfills, wetlands, agriculture), pyrogenic (biomass burning) and thermogenic sources (fossil fuel reservoirs). The most important sink of CH_4 is reaction with the hydroxyl radical (OH) in the troposphere (Vaghjiani and Ravishankara, 1991), which produces formaldehyde (HCHO) that is subsequently photolyzed or oxidized to yield CO and eventually CO_2. In addition to climate implications, CH_4 also has air quality implications through its role in NO_x catalysed ozone formation in the troposphere, especially in areas with large sources of CH_4. Of recent interest are wintertime rapid ozone formation events (OFEs) seen in regions of intense oil and gas extraction (Pinto, 2009;Schnell et al., 2009) that are associated with snow coverage (Edwards et al., 2013), shallow boundary layers (Schnell et al., 2016), high levels of ozone precursors and enhanced photolysis of HCHO and other carbonyls under radical limited conditions (Edwards et al., 2014).

The growth of the atmospheric burden of CH_4 increased in the post industrial revolution, slowed in the 1980's and 90's (Worthy et al., 2009), paused between 1990-2007 but has increased again starting in 2007, with an atmospheric growth rate of $\sim 0.4\%$ yr^{-1} from 2007-2014 in the northern hemisphere (Hausmann et al., 2016). Satellite observations have suggested a 30% increase in CH_4 emissions in the USA during 2002-2014 (Turner et al., 2016). The 2009-2014 trend in CH_4 mixing ratios and tropospheric columns of ethane was attributed to oil/gas production in the USA (Helmig et al., 2016) and recent increases in tropospheric columns of ethane and methane have suggested the global oil and gas sector to be partially responsible (Hausmann et al., 2016). Contrasting this, a recent study suggests that North American CH_4 emissions have been flat from 2000-2012 (Bruhwiler et al., 2017) and there is still ambiguity in the source versus sink role for the recent increase in atmospheric CH_4 (Turner et al., 2017). The above uncertainties underline a need for better quantification of anthropogenic emissions of CH_4 to the atmosphere and motivate the current study.

Emission inventories can quantify the contributions of specific sources to the atmosphere. However, bottom-up inventories benefit from top-down measurements and validation (Fujita et al., 1992), due to the difficulty in identifying all possible points of emission and quantifying all emissions in a large complex source (e.g., a city or a facility). Top-down measurements of various types have long been used in the validation of emission inventories and emission models including comparison of surface based pollutant profiles and ratios (Fujita et al., 1992;Jiang et al., 1997;Fujita et al., 1995), source-receptor methods (Scheff and Wadden, 1993;Fujita et al., 1995;McLaren et al., 1996), aircraft based flux measurements (Mays et al., 2009), measurement/modelling hybrid methods (Allen et al., 2004;Shephard et al., 2015) and satellite measurements (McLinden et al., 2012;McLinden et al., 2014;Turner et al., 2016;Kort et al., 2014;Jacob et al., 2016). Multiple studies have suggested underestimation of CH_4 emissions from natural gas infrastructure (Brandt et al., 2014;Hendrick et al., 2016). Several recent aircraft studies using mass balance approaches have quantified CH_4 emissions in oil and gas regions and compared these to inventory emission rates and/or leakage rates (Karion et al., 2013;Peischl et al., 2013;Karion et al., 2015;Peischl et al., 2015;Peischl et al., 2016;Lavoie et al., 2015). Other studies have used top-down satellite measurements to quantify emission of CH_4 in oil and gas regions (Schneising et al., 2014;Kort et al., 2014). As such, top down measurement of methane emissions and comparison with bottom up inventories can make a significant contribution to our understanding of the sources of CH_4.

In this study we quantify total emission rates of CH_4 from facilities in the Athabasca Oil Sands Region (AOSR) of Alberta in the summer of 2013. Alberta has large deposits of oil sands, an unconventional viscous mixture of bitumen, sand, silt, clay, water and trapped gases (Stringham, 2012). Canada has proven reserves of 1.69×10^{11} barrels of oil (2.7×10^{13} litres), third largest in the world, 97% of which are located in the oil sands [Orbach, 2012]. Approximately 82% of the oil sands are located in the AOSR north of Fort McMurray with 20% located in near surface deposits (depth < 100m) that can be mined using open pit techniques and the remainder located in deeper deposits requiring underground in-situ extraction. In both cases the oil must be separated from sand requiring the use of hot water or steam froth treatment, and organic solvent diluents (naphtha or paraffin) are used to help separate water and solids and/or to decrease the bitumen viscosity. For surface mining processes, once the bitumen is

separated, process water containing unrecovered organic diluents is recycled but some is discharged in large tailings ponds open to the atmosphere for further remediation. Oil extraction in the AOSR is unique in that unlike other oil and gas regions, CH_4 is not the primary economic commodity being extracted, but is an unintended by-product. In particular, a significant fraction of the CH_4 is not

5   associated with fossil fuel reserves, but is emitted from the tailings ponds (Small et al., 2015). The factors giving rise to the release of CH_4 from these ponds are complex but include the organic and inorganic chemical composition of the ponds, the diversity and types of microbial communities, especially methanogens, as well as the age of the ponds. It is reported that it took 20 years and 15 years for the largest ponds at Syncrude and Suncor respectively, to show evidence of methane bubbling from

10   the surface (Small et al., 2015). Additional fugitive CH_4 is associated with the gaseous component of the oil sand along with other gases (Strausz, 2003;Johnson et al., 2016) that are released during overburden removal, open pit mining and/or subsequent processing.

In the summer of 2013, an intensive ambient air measurement campaign took place in the AOSR with both ground and airborne components in support of the Joint Oil Sands Monitoring (JOSM) Plan

15   (JOSM, 2012). The airborne measurements were conducted to address four objectives: i) to measure and quantify air emissions from the oil sands mining facilities, ii) to study the downwind physical and chemical transformation of pollutants emitted, iii) to provide spatio-temporal measurement of pollutants suitable for intercomparison with simultaneous satellite nadir overpasses in the region, and iv) to support air quality model prediction capabilities. In this paper, we report CH_4 emissions from industrial

20   facilities in the AOSR based on the airborne campaign. We applied the Top-down Emissions Rate Retrieval Algorithm (TERRA) mass-balance approach (Gordon et al., 2015) to determine total CH_4 emissions rates from each of the major industrial facilities, as well as a second mass-balance approach using downwind flight tracks to spatially separate CH_4 emissions from different sources in each facility. Emissions rates of CH_4 are determined for the five major facilities in the region: Syncrude Mildred

25   Lake (SML), Suncor Energy OSG (SUN), Canadian Natural Resources Limited Horizon (CNRL), Shell Albian Muskeg River and Jackpine (SAJ) and Syncrude Aurora (SAU). These results are the first source-attributed emissions estimates for the facilities in the AOSR, obtained by identifying and characterizing plume origins according to signatures of chemical tracer species.

Experimental

2.1 Instrumentation

An array of instruments for the measurement of trace gases, aerosols, meteorological and aircraft state parameters were installed aboard the National Research Council of Canada Convair 580 research

5   aircraft. Measurements of CH_4, CO_2, CO and H_2O were made using a cavity ring-down spectrometer (Picarro G2401-m) at an interpolated rate of approximately 0.5 Hz with a flow rate of ~435 sccm min^{-1}. The precision of the CH_4 measurement was 2 ppb, and the uncertainty of the measurement at background (~ 1.9 ppm) was 3.3 ppb (@2 sec). The instrument was calibrated six times before, during and after the project using two standard reference gases traceable to NOAA GMD standards. Methane

10   mixing ratios are reported throughout as dry mole fractions in the paper. Necessary parameters for emissions estimation included Temperature (T), measured using Rosemount probe, Dewpoint temperature (T_d), measured with an Edgetech hygrometer, and pressure (P), measured with a DigiQuartz sensor. The three-component wind speed (U_x, U_y, U_z) was derived from a Rosemount 858 probe, GPS and Honeywell HG1700 inertial measurement unit. The uncertainty of horizontal and

15   vertical winds on the aircraft are 0.6 and 0.4 m/s respectively (Williams and Marcotte, 2000). Geospatial information (latitude, longitude, ellipsoid height altitude) was measured by GPS.

Nitrogen oxides (NO, NO_2 and NO_y) were measured with a modified trace level chemiluminescent analyser (Thermo Scientific Model 42i-TL). A molybdenum converter (325 °C) was used to convert NO_y species to NO and an NO_2 specific converter (Droplet Measurement Technologies) was used to

20   convert NO_2 to NO. Detection limits for NO, NO_2, and NO_y were determined to be 0.08 ppb (1 sec), 0.20 ppb (2 sec), 0.09 ppb (1 sec) respectively. Sulfur dioxide (SO_2) was measured with a pulsed UV fluorescence analyser (Thermo Scientific: Model 43i-TLE) with a detection limit of 0.7 ppb (1 sec). Ambient air was drawn in through filtered 6.35 mm (1/4") diameter PFA tubing taken from a rear-facing inlet located on the roof toward the rear of the aircraft. Measurements of NO, NO_2, NO_y and SO_2

25   were made downstream of a constant pressure inlet system maintained at 770 mmHg with a total flow rate of 5 Lpm. In flight zero and background determinations were made several times throughout each

flight and the analysers were calibrated multiple times during the study against National Institute and Standards Technology (NIST) certified reference gases.

Refractory black carbon mass (rBC), was measured with a Droplet Measurement Technologies (DMT) Single Particle Soot Photometer (SP2). Ambient air was subsampled from the main aerosol flow that was brought into the main cabin with a forward-facing shrouded diffuser isokinetic aerosol inlet (Cheng et al., 2017). Benzene, toluene, ethylbenzene and xylenes (BTEX) were measured by a Proton Transfer Reaction time-of-flight Mass Spectrometer (PTRMS) from the main gas inlet. Further technical details are provided elsewhere (Li et al., 2017). The delay time of each instrument was determined experimentally and through calculations based on sample flow rates and inlet volumes. Total delays are contributed to by the response time of the instruments (1–3 sec) as well as the volume of sampling tubing. Data were adjusted to account for the total delay times of 2-6 sec to spatially and temporally synchronize the different measurements (Picarro delay time = 6 sec). The average speed of the aircraft was 90 ms^{-1} during the research flights, thus providing a spatial resolution of 90-270 m based upon the internal response time of each measurement.

2.2 Aircraft Flights

In total, there were 22 flights with 84 hours of measurements in the AOSR between August 13 and September 7, 2013. The flights were designed for three purposes; measurement of pollutant emissions from facilities (Gordon et al., 2015;Li et al., 2017), measurement of pollutant transformation downwind of the AOSR (Liggio et al., 2016) and comparison with satellite overpasses (Shephard et al., 2015). Thirteen flights were dedicated to quantifying facility emissions with a minimum of two flights for each of the SML, SUN, CNRL, SAJ and SAU facilities. CH_4 above background was not detected during the 2013 flights targeting the Imperial Kearl Lake (IKL) facility, which was not in full production mode at the time (but has since expanded significantly), nor from the Suncor Firebag in-situ operation. We did detect CH_4 above background suspected to originate from the Suncor MacKay River operation (west of SML). We were not able to quantify this source separately, however emissions from this source are included in one measurement of the total emissions from all mining facilities in the AOSR using a wide downwind screen (see section 3.4 and Fig. 7). Several other flights are not included in the analysis due

to unfavourable meteorological conditions including wind shear problems or insufficient numbers of transects. In total, seven flights were found to be suitable for identifying and quantifying emissions of CH_4 from the facilities. Figure 1 displays several of the flight tracks over and downwind of the target facilities north of the Fort McMurray airport.

5   The flight patterns designed for the quantification of emissions rates were of two types: i) screen flights, wherein the aircraft flew transects perpendicular to the plume downwind of one or more facilities, and ii) box flights, wherein the aircraft flew transects at multiple heights around a single target facility in a box-type pattern (Gordon et al., 2015;Li et al., 2017). The transects were performed at heights from 150 to 1370 m above ground level (agl), complemented by vertical profiles designed to determine the height

10 of the planetary boundary layer (PBL) and to compare with ground based measurements.

2.3 Mass Balance Approaches for Determining CH_4 Emissions

Following the TERRA methodology (Gordon et al., 2015), the time resolved measurements were interpolated using covariance kriging to produce a 40 m (horizontal, s) by 20 m (vertical, z) contiguous screen of CH_4 mixing ratios. Within TERRA, the CH_4 mixing ratios are extrapolated from the lowest

15 transect (~150 m agl) to the surface using a constant, linear or half-gaussian extrapolation, depending on the type of source and the boundary layer conditions at the time. Uncertainty estimates (see section in Supplemental) are included according to the various types of surface extrapolation applied. Interpolated matrices were constructed for measurements of air pressure (P_{air}) and temperature (T_{air}) in order to determine the air mass balance within the box and to convert mixing ratios to mass densities. Spatially

20 equivalent interpolations of wind velocity perpendicular to aircraft motion ($U_\perp$) were created from the vector components of wind speed and direction measurements.

Emissions rates were determined according to the two different mass-balance approaches for screen and/or box flight patterns. Horizontal tracks at multiple altitudes flown perpendicular to the general wind direction produce a virtual screen downwind of the target that is intercepted by emission plumes

25 from the facilities. Fluxes of CH_4 moving through each 40 x 20 m (s × z) pixel can be determined from the interpolated matrices and integrated for a dimensional s by z target area according to Equation 1,

$$E_{Screen} = \iint_{S1,z_b}^{Sn,z_t}([CH_4] - [CH_4]_B) \times U_\perp \, ds \, dz \qquad \text{(Eq. 1)}$$

where ([CH_4] – [CH_4]$_B$) is the enhanced mixing ratio of CH_4 above background, U_T is the horizontal wind velocity perpendicular to the screen (e.g. $U \times \sin \theta$, θ = angle between wind vector and airplane vector), s_1 and s_n are the horizontal integration limits along the screen transect, z_b and z_t are the bottom and top vertical integration limits. Background mixing ratios of CH_4 were determined from the outside edges of the screens away from plume sources. Because [CH_4]$_B$ varies with height, a vertically variant background profile was subtracted from each vertical measurement column, an approach used in other mass balance determinations (Cambaliza et al., 2014;Karion et al., 2013). Example vertical profiles of [CH_4]$_B$ (z) for each day are included in Figure S1 (Supplemental Information). The simple mass balance approach represented by Eq.1 can be applied to individual downwind screens from other flight paths (i.e. box flights) to determine CH_4 emissions from specific sources within a facility.

The second mass balance method used in this paper is to apply the full box-model TERRA algorithm (Gordon et al., 2015), to compute total emissions from all sources within a box, where the box is made up of multiple (4-6) screens forming a polygon encompassing a facility. This more rigorous mass balance approach used for calculating total emissions from a facility is represented by Equation 2

$$E_{Box} = E_{CH} + E_{CHT} + E_{CV} + E_{CVT} + E_{CM} \qquad \text{(Eq. 2)}$$

where E_{Box}, the total emissions rate from all sources within a box, is the sum of the horizontal advective and turbulent fluxes (E_{CH} and E_{CHT}), vertical advective and turbulent fluxes (E_{CV} and E_{CVT}), and the change in CH_4 mass within the box volume (E_{CM}). Because the box includes screens that are downwind, upwind and lateral to sources, incoming (background) and outgoing (background + source) fluxes are determined as a part of the horizontal flux terms (E_{CH} and E_{CHT}). Vertical fluxes through the box top, normally ignored in the conventional mass balance approaches (Eq. 1), are estimated according to the conservation of air mass within the box volume and the mixing ratio at the top edge of the box. E_{CM} is estimated according to the time derivative of the ideal gas law, based on measured changes in pressure and temperature over the flight time (see Gordon et al., 2015 for a full discussion).

The advantage of the box approach (Eq. 2) over the screen approach is a more precise estimate of total emissions by accounting for incoming and outgoing fluxes and meteorological effects within a volume. However, this flight pattern takes more time to completely surround a target facility. The advantage of the screen approach (Eq. 1) is the computation of CH_4 fluxes per pixel, which can thus be used to

5   spatially integrate individual emission plumes of arbitrary shapes when the sources can be spatially resolved. Studies applying aircraft mass-balance methods have used each of single-height transect (Karion et al., 2013;Peischl et al., 2016), single screens (Cambaliza et al., 2014;Walter et al., 2012), spiral (Wratt et al., 2001;Gatti et al., 2014), and full box flight paths (Gordon et al., 2015) for the purpose of determining emissions rates and characterizing meteorological conditions. The aircraft

10 flights presented contained various segments of tracks that allowed applications of all the above methods. In this work we apply a systematic approach deriving information from each of these techniques for a comprehensive top-down characterization of CH_4 sources and emissions in the region. Single-height transects are used to determine source chemical signatures by identifying CH_4 enhancements and their associations with other trace-gas species. Vertical profiles are used to determine

15 the PBL height throughout flights. Single screens are used to determine CH_4 emissions rates (Eq. 1) for facilities and their individual sources when plumes are spatially resolved. Box flights are used to determine total CH_4 emissions from facilities at a lower uncertainty (Eq. 2) and source-specific emissions are determined where possible (Eq. 1).

20 The summer time emission rates measured in this study are reported in units of metric tonnes CH_4 per hour, an appropriate unit given the duration of the flights (i.e., a few hours). We do not attempt to derive annual emissions as the assumptions needed to do so are highly uncertain without measurements in other seasons for a volatile species such as CH_4. However, we do make a first order comparison to emission inventories and other studies that report emissions on an annual basis by downscaling the

25 annual emissions to hourly emission rates using an assumption of a constant temporal factor throughout the entire year. This is appropriate for emission inventories that are based upon measurement of emissions or emission factors in summer, that then upscale their emission rates of CH_4 to annual emissions using a constant temporal factor assumption (e.g., GOA, 2014). However, the assumption of

a constant temporal factor is far from being validated and further measurements in different months are needed to understand the potential for seasonal variability of fugitive emissions of CH_4.

Previous work shows the box approach has a demonstrated uncertainty of 25-27% for total emissions of CH_4 from a facility in the AOSR (Gordon et al., 2015). Uncertainty due to extrapolation of CH_4 mixing ratios from the lowest height measurements to the surface was estimated to be 15% and 26% in that study. In contrast, screen approaches used in other studies have estimated uncertainty in the range of 30-50% (Cambaliza et al., 2014) with the main sources of error attributed to the reliability of plume characterization and the stability of meteorological conditions. In this study, uncertainties in both the box and screen estimates are reduced through i) a high number of transects over a wide vertical range to accurately characterize vertical structure in the PBL, ii) reliable measurements of background CH_4 (or incoming fluxes for boxes), iii) measurements of the PBL height to account for meteorological variance, and iv) measurements within time periods of minimal PBL change. In addition, the enhancement of CH_4 in the plumes downwind of the facilities and high precision of the Picarro instrument minimize uncertainties in plume characterization and background CH_4. The overall uncertainty for computed CH_4 emission rates for an individual determination was estimated to be less than 30% (see Supplemental for a complete evaluation and discussion of uncertainties).

3. Results and Discussion

3.1 Identification of Sources of CH_4

Two example flights from three different facilities (SML, SUN and CNRL) are presented to demonstrate CH_4 emissions in the AOSR are mainly from three source types: open pit mining, tailings ponds, and facility activities. Emissions from the remaining two facilities (SAJ and SAU) were shown to be primarily open pit mining. Source categories were identified by measurements of CH_4, NO_y, BTEX, and rBC. Figure 2 shows measurements from one low-level transect of a screen flight on Aug 16, 2013 (9 transects in total). This transect was flown at a height of approximately 150 m agl downwind of the SML and SUN facilities, showing clear separation of emission sources from the two

facilities. Four distinct plumes are visible, labelled A-D, with linear air parcel back-trajectories indicated in red arrows. Back trajectories were determined using the wind speeds and wind directions measured on the aircraft at flight level from the positions of maximum CH_4, back extrapolated as a general indicator of plume origin. This methodology creates a western bias in our plume origins. A

5   more careful analysis of surface winds at several meteorological stations in the local vicinity at the time of the aircraft transect shows that surface wind directions were from ~ 140-180° (SE) compared to the flight level winds, ~220° (SW). The low level surface winds are likely channelled by the river valley, which runs in a SE to NW direction. Thus the trajectories of air masses originating at the surface and mixing upwards have a clockwise rotation, a very local effect, placing the actual plume sources further

10   east than the linear tracks show in Figure 2. Plume A shows a maximum mixing ratio of 2.68 ppm CH_4, an enhancement of ~ 0.58 ppm above a background of ~2.1 ppm on this day in this region. This enhanced CH_4 is associated with values of 2.3 $\mu g/m^3$ rBC and 47 ppb NO_y. The simple linear wind back-trajectory places the origin of the air mass near the western edge of open pit surface mining activity ~100-min earlier, although as mentioned the actual source is likely slightly east of that location

15   due to the clockwise rotation of the plumes. The combination of rBC and NO_y is indicative of exhaust of heavy hauler diesel trucks that operate in open pit mines. However, significant CH_4 emissions are not expected from the truck exhaust, as emissions factors of CH_4 from off-road gasoline and diesel combustion indicate that the CH_4/CO_2 emission ratio would be 1 to 2 orders of magnitude lower (Environment Canada, 2015) than the $\Delta CH_4/\Delta CO_2$ observed in this plume (0.58 ppm CH_4 / 16.1 ppm

20   CO_2). Disturbance of the oil sands at the mine faces by the trucks is a well-known source of CH_4 with minor emissions of CO_2 and other VOC's (Strausz, 2003) as well as intermediate volatility organic compounds (Tokarek, 2017). Thus, Plume A is interpreted to be a combination of heavy truck exhaust, indicated by the presence of rBC and NO_y, that spatially overlaps with the mine face source of CH_4. Plume D shows a similar chemical profile with a maximum CH_4 of 2.40 ppm, ~ 0.30 ppm above

25   background, associated with elevated levels of NO_y (40ppb) and rBC (1.5 $\mu g/m^3$). The back-trajectory for Plume D is in agreement with an origin at one of two locations of open pit mining activity at SUN. The two plumes show a similar $\Delta NO_y/\Delta rBC$ ratio within the range of 15-30 ppb per ug/m^3. We

consistently measure this profile of NO_y and rBC enhancements from active mines across all five facilities.

Plume B (Fig. 2) shows the highest CH_4 mixing ratio at 4.19 ppm, an enhancement of ~2.09 ppm above
5   background. The back-trajectory from the position of the maximum CH_4 places the air mass over the western edge of Mildred Lake Settling Basin (MLSB) tailings pond ~ 20 minutes earlier. The CH_4 enhancement occurs simultaneously with a decrease in NO_y and rBC and an enhancement of total BTEX from ~0 ppb to a maximum of 7.6 ppb. Tailings ponds are known to contain significant quantities of BTEX compounds due to waste streams of mature fine tailings containing naphtha diluent
10   flowing into the pond (Small et al., 2015). This is similar to the chemical profile observed in Plume C, with a back-trajectory placing the air mass over one of several possible SUN facility tailings ponds shown in Figure 2 (Ponds 6, Pond 5 and Pond 2/3 in figure Small et al, 2015). This indicates the presence of CH_4 emissions from multiple tailings ponds. Anaerobic digestion of organic matter in the tailings pond is the primary mechanism for the production of this biogenic CH_4 (Siddique et al., 2012).
15   For Plume C the measured mixing ratio enhancements are 0.25 ppm CH_4 and 2.3 ppb of BTEX. The lower CH_4 enhancement compared to Plume B suggests less CH_4 is emitted from this pond, in agreement with Small et al (2015). The peak-to-peak CH_4/BTEX ratios from Plume B and Plume C are ~300 ppb ppb^{-1}, and ~100 ppb ppb^{-1} respectively. The difference in measured inter-facility CH_4/BTEX ratios could arise from a number of factors including different pond ages, history, depth, methanogenic
20   behaviour, or use of different diluents in each facility. The in-plume correlations of CH_4 with the associated tracers (NO_y, rBC and BTEX) for each of the Plumes identified in Figure 2 are shown in Figure S2 (Supplemental Information).

Our observations are qualitatively consistent with pond-specific industry reported CH_4 emission factors,
25   which present SML and SUN Ponds 2/3 (Small et al., 2015) as the highest CH_4 emitting tailings ponds in the region. We consistently measured relative enhancements from plumes downwind of SML and SUN according to the pattern of Plumes B and C in Figure 2, demonstrating the feasibility of using BTEX compounds as tracers for CH_4 being emitted from tailings ponds. We expect that BTEX would

be greatly reduced from the tailings ponds of those facilities using paraffinic froth treatment (e.g., SAJ) instead of naphtha. In such cases, light hydrocarbons could in principle be used as tracers for the tailings ponds emissions of CH_4. However, we did not detect methane plumes above detection limit that were distinct from the open pit mining plumes of CH_4 associated with rBC and NOx for any facilities other than SML and SUN.

Elevated plumes from facility stacks are the primary sources of SO_2 in the AOSR due to the bitumen upgrading process. Hence, a significant enhancement of SO_2 can be used as a tracer for plant or stack CH_4 sources. However, this is not measured at the height shown in Figure 2, which shows a maximum SO_2 of only 5 ppb for this transect between Plumes C and D at 150 m agl. For the same flight (Figure 2), maximum SO_2 was 131 ppb for a transect ~350 m above ground, with an associated narrow peak of CH_4 with maximum mixing ratio of 2.11 ppm. While higher-altitude SO_2 plumes were frequently measured downwind of various facilities over the course of the aircraft campaign, in most cases no significant CH_4 enhancements were observed in these plumes. A similar case is discussed in Section **3.2** where we show the full range of vertical measurements and a lack of enhanced CH_4 in the SO_2 plume. Ground-level CH_4 from tailings ponds and open pit mine faces therefore dominate the CH_4 emissions in the region, with minor contributions from industrial plants.

We next compare the profiles from SML and SUN to a third facility, CNRL Horizon. Figure 3 shows a similar transect at ~150 m agl from the Sep 02 flight in the vicinity of CNRL. The bottom panel of Figure 3 shows that there was considerable wind divergence at this time (see back trajectory arrows for A, B, C). This wind divergence was also present in the next pass of the aircraft on the south side of CNRL at a height of 300m (not shown). While this divergence aids in the visualization of source separation, they invoke uncertainty in the mass balance determinations. The emission rates on Sept 02 were determined using ten transects from a flight much earlier in time than that shown in Fig 3., when the winds were more consistent in direction (NNW).

While Plume A shows a small enhancement of ~1 ppb BTEX downwind of the tailings pond, in contrast to SML and SUN no significant CH_4 was associated with it. This is consistent with the pond-specific emission factors presented in Small et al. (2015) that do not list the CNRL tailings pond as a significant source of CH_4. The primary Plume B included a CH_4 mixing ratio up to 2.24 ppm (enhancement of

5 ~0.34 ppm above background) associated with 12 ppb NO_y and 0.7 ug/m^3 rBC downwind of the CNRL mine. Consistent with the previously described open pit profile and the back trajectory, we identify Plume B as an open pit mining source of CH_4. A secondary Plume C was measured with maximum CH_4 of 2.02 ppm (enhancement of ~0.12 ppm) east of the open pit mine. The lack of associated species does not relate the origin of Plume C to either a tailings pond nor an open pit mine source of CH_4. The plume

10 is downwind of the main CNRL plant and closer in horizontal proximity to SO_2 plumes measured during higher altitude transects. This suggests a CH_4 source near the main plant that could originate from venting or flaring activity, electricity cogeneration using natural gas or natural gas leakage. Thus the primary source of CH_4 from the CNRL facility is open pit surface mining activity with a secondary undetermined source from the main plant.

15

Source profiles of CH_4 are further compared to measurements of ethane (C_2H_6). Source-attribution studies for CH_4 commonly use higher ethane-to-methane ratios (EMRs) as a signature for oil and gas emissions, on both a regional (Peischl et al., 2016) and global (Hausmann et al., 2016) scale, while low EMR ratios can be indicative of microbial sources of methane that do not emit ethane (agriculture,

20 landfills, wetlands, etc.) (Smith et al., 2015). C_2H_6, along with other VOC's, was measured from 20-second grab samples collected in 3-L Summa canisters. The VOC's were analysed offline using GC-MS and GC-FID methods described elsewhere [Li et al., 2017]. Table 1 shows C_2H_6 measurements from three different flights (Aug 14, Aug 16 and Sep 02) when canister sampling overlapped with the plume descriptions listed previously. In all cases shown, enhancements of C_2H_6 above background (0.8

25 – 1.5ppb) were in the range of only 1-2 ppb, normally the highest enhancements for each flight (within 1 ppb of 95th percentile). The small emissions rates of ethane (EMRs <1.4%) across flights contrasts with the high EMRs (i.e. 40-50%) seen for conventional oil and gas fields in other regions of North America (Peischl et al., 2016;Smith et al., 2015) and is lower than all the possible EMR source

scenarios tested in Hausmann et al. (2016). The problems associated with determining EMR ratios from a combination of continuous CH_4 measurements and discrete canister sampling of ethane from aircraft have been highlighted recently, where it was shown that actual EMR ratios determined in this way can be off by up to a factor of two (Smith et al., 2015). Thus the limited EMR data shown in the Table 1 are

5   not intended to be a comprehensive measure of EMR in the AOSR but simply to support the conclusion that the major sources of methane from the facilities in the AOSR are microbial in nature without a significant co-emission of ethane. The low EMRs are consistent with previous measurements in the region (Simpson et al., 2010) and are an indication of the unique character of unconventional bitumen sources. As such, global estimates of the relative contributions of oil and gas emissions to decadal

10   increases in atmospheric CH_4 that are based on C_2H_6 and CH_4 measurements in the free troposphere (Hausmann et al., 2016) would not capture AOSR emissions due to the low C_2H_6 emissions in this region.

3.2 Quantification of CH_4 Emission Rates from Sources

The source chemical profiles in section 3.1 can be used in combination with the screen mass-balance

15   method (Eq. 1) to isolate and quantify categories of AOSR emissions. As an example, we show the Aug 14 flight surrounding the SML facility, which consisted of a box and screen path flown in rapid succession. Figure 4 shows an image of the interpolated aircraft measurements from the box path creating a contiguous mesh superimposed on a map of the region. Winds were from the south at 186 ± 48 degrees over the course of the day. Three distinct ground-based plumes of CH_4 are visible, a primary

20   plume (Plume N) on the northern screen (~6500 m wide) exiting the box, a secondary plume (Plume NW) at the northwest corner (~7000 m wide) exiting the box and a smaller plume (Plume E) on the eastern screen (~3000 m in width) entering the box from outside the SML facility boundary. The lowest aircraft transect was at a height of ~150 m agl, with maximum CH_4 mixing ratios of 3.00 ppm, 2.60 ppm and 2.63 ppm respectively for the three plumes. Mixing ratios of CH_4 below 150 m agl, are based

25   on a linear extrapolation of interpolated pixels to the surface, corresponding to maximum surface mixing ratios of 3.48, 3.17 and 3.06 ppm for the primary (N), secondary (NW) and tertiary (E) plumes respectively. Extrapolation to the surface is the primary source of uncertainty for surface sources in this

method, however the uncertainty can vary between flights depending on the meteorological conditions (Gordon et al., 2015). As a part of our uncertainty analysis in the Supplemental material, we have included an uncertainty associated with the differences in emission rates that arise from the use of linear, constant and half-Gaussian extrapolations in the calculations.

5

Unwrapped curtain plots of CH_4, BTEX, NO_y, rBC and SO_2 from the Aug 14 box flight (Fig 4) are shown individually in Figure 5, projecting the 3-D virtual box onto a 2-D grid. The same three plumes from Fig 4 are highlighted by dotted boxes in red (N screen), yellow (NW corner), and black (E screen). The red and yellow boxes show sources originating from within the SML facility and the black boxes

10 show a source originating outside of the SML boundaries and entering the box from the east. The largest SML CH_4 plume is associated with > 10 ppb BTEX and the absence of rBC and SO_2, with some NO_y (~20 ppb). This is consistent with the chemical signature associated with tailings pond emissions discussed previously. The NW plume is associated with >60 ppb of NO_y and up to 5 $\mu g/m^3$ of rBC, with minimal BTEX and SO_2, consistent with the expected chemical signature from open pit surface mining.

15 The smaller plume on the E screen is associated with elevated BTEX and CH_4 and is likely a plume from one of the SUN tailings ponds as the winds indicate the plume is entering the box. The elevated plume in Fig 5 (orange circles) with ~100 ppb SO_2 and ~30 ppb of NO_y is traced to the SML upgrader activities, but with no enhancement of CH_4 above background on this day. A second NO_y plume is visible at the north-eastern corner of the box, not associated with any of the identified CH_4 source types.

20 This NO_y plume likely originates from traffic on the main highway that passes between the SML and SUN facilities and/or trucks and other vehicles operating in and around the main SML facility.

Boundaries of the plumes from separate sources are estimated using the tracer species listed in Fig. 5 by evaluating where the chemical signatures reached background levels. However, the SML tailings pond

25 and open pit mine plumes were not completely resolved from one another, overlapping within a range of ~800 m. The uncertainties in the emission rates due to plume overlap were estimated by contracting and expanding the horizontal integration boundaries (s) by 800 m on each side (a total of ±1600 m) as part of the sensitivity analysis. A vertically varying background profile ($[CH_4]_B(z)$) is determined using

data from the upwind southern screen, as mentioned previously. Using a spatially identical screen of

perpendicular wind $U_\perp(z)$, the fluxes are determined through each pixel and the total source emission is

calculated by integrating the pixels within the plume boundaries (Eq. 1). CH_4 emissions rates are

computed to be 6.4 ± 1.2 metric tonnes per hour (tonnes hr^{-1}) for the SML main tailings pond and $2.7 \pm$

5   0.6 tonnes hr^{-1} for the SML open pit mine source. It is possible that the CH_4 plume from the SML

tailings pond includes CH_4 emissions from the main SML plant facility (flaring, venting, natural gas

leakage, etc.) that cannot be spatially separated from one another due to their proximity, however we

anticipate the magnitude of these emissions are minor and captured within the error intervals listed.

10   This screen-based mass-balance approach for determining specific source emission rates (Eq. 1) is

applied to flights with appropriate conditions for plume separation. Mean emissions rates of CH_4 from

specific sources within the facilities SML, SUN, CNRL, SAU and SAJ are shown in Figure 6. SML

emissions rates are the average of three mass-balance flights over two days (two on Aug 14 and one on

Aug 16). Two flights on separate days were used for each of the SUN (Aug 16 and Aug 29), SAJ (Aug

15   21 and Sep 06) and SAU (Aug 29, Sep 06) facilities. One CNRL flight (Sep 02) had northerly wind

conditions showing plume separation on a southern screen. No significant daily variability is observed

as the emissions rates for the same source agree within error. Duplicate and triplicate estimates for the

same source are combined using an error-weighted uncertainty (Supplemental). SML and SUN had

significant open-pit mining emissions of CH_4, 2.8 ± 0.4 tonnes hr^{-1} and 1.8 ± 0.2 tonnes hr^{-1}

20   respectively, and were the only facilities with tailings ponds emissions above detection limit, 6.4 ± 0.8

tonnes hr^{-1} and 2.4 ± 0.3 tonnes hr^{-1}. CNRL had open-pit mining emissions (2.6 ± 0.7 t/hr) and

significant emissions originating from the main plant facility (1.0 ± 0.3 t/hr). Plumes of CH_4 from SAJ

and SAU were only attributed to open-pit emissions, 1.2 ± 0.2 t/hr and 1.4 ± 0.2 t/hr respectively.

25   The plume-targeting screen mass balance method described here is unable to resolve emissions of CH_4

from multiple sources not characterized by the chemical profiles described in Section 3.1 if they cannot

also be spatially separated. Because spatial s and z constraints are manually chosen by plume

boundaries from chemical profiles, minor emissions may contribute to overestimation of the emissions

from an individual source when highly coincidental in space such that the sources are not separable. For example, the emissions from the main plant were identifiable in the case of CNRL due to the separation and orientation of the plant, the open pit and the tailings ponds with respect to the winds. This was not the case for the other major facilities in the AOSR where many of the sources were highly coincidental

5 in space. It is possible, and even likely, that other major facilities in this study also have CH_4 emissions from their main plants (venting, cogeneration, natural gas leakage, etc.) that are identified as tailings pond emissions or open pit emissions due to close proximity and our inability to deconvolute the sources spatially or chemically. However, we expect that the total emission rates of CH_4 from each facility are still accurate.

10

Emissions rates from each flight and individual sources (where possible) using the screen mass balance method are tabulated in the supplemental (Tables S1-S5). We did not measure a detectable tailings pond source of CH_4 from CNRL, SAJ and SAU. Associated enhancements of rBC and NO_y with CH_4 suggest that the CH_4 source from SAJ and SAU is also predominantly open pit mining. The results

15 using the screen mass balance approach (Eq. 1) are further verified in Section 3.3 using emissions rates for each facility determined from the box approach (Eq. 2).

3.2.1 Comparison to Fugitive Emissions Literature

Average open pit surface mining emissions from the five facilities are within a range of 1.2-2.8 tonnes hr^{-1} (Fig 6 and Table S1-S5). This shows some consistency in the nature of CH_4 release from open pit

20 mining activity in the region, with differences that may possibly be attributed to the size of the surface disturbance taking place and the intensity of the mining activity. Methane emissions from open pit mines were recently estimated using a bottom-up emissions factor approach by analysing the gaseous composition in the overburden and oil sand component of drill core samples (Johnson et al., 2016). Emissions factors of CH_4 were then scaled up according to the total mass of material mined or the total

25 bitumen produced. For 2013, Johnson et al. estimate total fugitive mining emissions in the region to be 21.4-46.0 ktonnes of CH_4 using total mined material, and 33.1-85.0 ktonnes of CH_4 using total mined bitumen. Our top-down approach estimates total fugitive emissions from open pit mining to be 9.7 ± 0.9

tonnes hr^{-1}, corresponding to 84.9 ± 7.9 ktonnes yr^{-1} CH$_4$ if constant temporal emissions are assumed. Agreement with the upper estimates in Johnson (2016), despite the uncertainty associated with extrapolation to annual emissions, suggests that their bottom-up emissions factors from gases in core samples may reliably predict real-world emissions provided there is accurate characterization of CH$_4$ in

5   the core samples over the entire disturbed area. This is reasonable considering that it would be expected that degassing of an extremely volatile gas such as CH$_4$ from the oil sands material would be quantitative in a short period of time after the ore is exposed or crushed.

From our 2013 measurements, only two facilities, SML and SUN, had significant emissions of CH$_4$

10   from tailings ponds. Tailings ponds emissions accounted for ~70% and ~58% of total CH$_4$ from SML and SUN respectively. This accounted for ~45% of total emissions in the AOSR. Recently, bottom-up area-weighted emissions factors of CH$_4$ from 19 major tailings ponds in the AOSR were provided for the year 2012 (Small et al., 2015). The top three emitting ponds reported were 'Mildred Lake Settling Basin' (MLSB) and the 'West In-Pit' (WIP) pond within SML, and 'Pond 2/3' (P23) within SUN.

15   These tailings ponds account for >96% of tailings ponds CH$_4$ in the region according to that study. This is qualitatively consistent with our measurements of CH$_4$ mainly from SML and SUN. Our method requires CH$_4$ plumes to be clearly enhanced above background, so trace amounts of CH$_4$ from ponds in the other three facilities were not detected. This could be related to differences in the chemical composition of the process streams being released into these ponds, or it could simply be due to these

20   ponds being younger in age, with insufficient time for the anaerobic methanogenic communities to be established (Small et al., 2015). We are unable to differentiate emissions from ponds within the same facility due to overlapping chemical profiles from ponds within close proximity. However, using the ratios of relative pond emissions rates within the same facility presented in Small et al. (2015), (i.e. MLSB contributes 92% to SML emissions, Ponds 2/3 contribute 85% to SUN), we can infer individual

25   pond emissions from our measurements assuming the relative contributions are accurate. The resulting emissions rates are 5.8 ± 0.8 tonnes hr^{-1} for MLSB and 2.0 ± 0.3 for Ponds 2/3. This ranks the MLSB tailings pond as the highest area source of CH$_4$ in the AOSR, followed by the open-pit mines in SML and CNRL, and fourth Ponds 2/3 in SUN. Total CH$_4$ from tailings ponds in Small et al. (2015) are

estimated to be 30.3 ktonnes of CH_4 per year, with 29.7 ktonnes of CH_4 from the SML and SUN facilities (~98%). Our total CH_4 emission rate determined for tailings ponds is 8.8 ± 0.9 tonnes hr[1], which corresponds to 77.1 ± 7.9 ktonnes yr^{-1} if a constant temporal factor is assumed. This is 2.3-2.9 times larger than the emissions inferred from the data in Small et al (2015), despite the uncertainty of extrapolation to an annual emissions rate. Our measurements suggest more work is needed to reconcile top-down and bottom-up CH_4 emissions.

3.3 Emission Rates of CH_4 from AOSR Facilities

Total emissions rates of CH_4 from each facility determined using the box mass balance method (TERRA) are tabulated in the supplemental (Tables S1-S5) along with the determinations using the screen approach. Where multiple screen estimates or multiple box estimates were available, uncertainty weighted ($1/\sigma^2$) averages were determined for each method for each facility and are summarized in Table 2. While the box method is in some cases based on the same downwind measurements as the screen approach, the two methods have several key differences (described in **2.3**) and are treated as independent estimates. In particular, the box method does not resolve specifically targeted, individual plumes and instead determines the net outgoing flux from the closed volume surrounding the facility. Thus, consistency between the two estimates is evidence that the primary sources of CH_4 from facilities in the AOSR are tailings ponds, open pit mines and facility emissions captured by the source characterization in sections 3.1 and 3.2. In general, the total emissions from each facility using the screen and box methods are in agreement within uncertainty, which adds confidence to the measured emission rates reported here. In the final row of Table 2, we calculate a weighted average emission rate for each facility using all screen and box measurements. The CH_4 emission rates from the facilities are 8.6 ± 0.9, 4.2 ± 0.4, 3.6 ± 0.5, 1.3 ± 0.2, and 1.5 ± 0.2 tonnes CH_4 hr^{-1} from the SML, SUN, CNRL, SAJ and SAU facilities, respectively.

3.4 Total Emissions of CH_4 from the AOSR

The total CH_4 emissions from the five mining facilities in the AOSR, obtained by summing the best estimates (i.e., uncertainty weighted average of multiple measurements, bottom row, Table 2) of the

individual facility emission rates is given in the final row and column of Table 2. The 5-facility total

emission rate of CH_4 is 19.2 ± 1.1 tonnes CH_4 hr^{-1}. A final independent estimate of total AOSR

emissions was obtained from a flight on Aug 16, utilizing an independent transect screen ~75 km wide

(Aug 16 Screen B) downwind of all major mining facilities in the AOSR (excluding Imperial Kearl

5   Lake and Suncor Firebag operations; but also inclusive of any emissions from Suncor MacKay River in-

situ facility). The details of this flight are given in Supplemental Table S6. The interpolated screen from

the Aug 16 flight (Total OS) is shown in Figure 7. The screen was constructed from 10 aircraft

horizontal transects from 250-900 m agl. Enhancements of CH_4 were measured over a wide horizontal

subrange of ~60 km of the entire ~75 km screen. Winds were perpendicular to the plane from the

10   southwest (225°), showing a large flux of CH_4 through the screen from upwind sources. The highest

measured mixing ratios of CH_4 were 2.67 ppm at the ~250 m (agl) transect. Background CH_4 in the

region was ~2.00 ppm taken as a vertical profile from the wings of the screen. Using the screen method

(Eq. 1), the emissions rate was determined to be 23.0 ± 3.7 tonnes CH_4 hr^{-1}, which represents the

emissions from all major facilities within the AOSR domain. This AOSR total is only slightly larger

15   than the previous 5-facility total emission rate of 19.2 ± 1.1 tonnes hr^{-1}, but not statistically so,

demonstrating the reproducibility of our measured estimates. It is entirely possible that there are other

minor sources of CH_4 included in this larger number from smaller industrial operators in the region,

trucks and vehicles on the main highway, and wetland emissions. In fact, the Canadian GHGRP

inventory (see section 3.5) indicates that there is an additional 0.13 tonnes CH_4 hr^{-1} emitted upwind and

20   0.17 tonnes CH_4 hr^{-1} emitted downwind of the aircraft screen (Fig 7) from minor industrial facilities

within the AOSR (both numbers downscaled from the facility reported annual emissions). The amount

of CH_4 emitted from vehicles on the highway though is expected to be smaller. The fact that the two

numbers are not statistically different supports the determination that the majority of the CH_4 in the

AOSR is emitted from the 5 major industrial facilities in the region. The two values are combined here

25   using an error-weighted uncertainty resulting in a final AOSR facility emissions estimate of 19.6 ± 1.1

tonnes CH_4 hr^{-1}, measured during a summertime period.

3.5 Comparison to Emission Inventories

Emissions of anthropogenic greenhouse gases are estimated by ECCC in Canada's GHG Inventory, which forms the basis for Canada's annual report to the United Nations Framework Convention on Climate Change , UNFCCC (ECCC, 2016). Currently, industrial facilities that emit more than 50

5 ktonnes CO_2eq yr^{-1}are required to report their emissions annually to ECCC using the Greenhouse Gas Reporting Program (GHGRP), which is Canada's legislated, publicly accessible inventory of facility-reported greenhouse gas (GHG) data (ECCC, 2017b). Although the GHGRP inventory data is not necessarily used in Canada's GHG Inventory, changes are being proposed to expand monitoring requirements in the GHGRP, including lowering the reporting threshold to 10 ktonnes CO_2eq yr^{-1} in

10 order to enable direct use of the reported data in Canada's GHG Inventory (ECCC, 2017a). Emissions of CH_4 from all five major oil sands facilities discussed in this paper are present in the GHGRP Emissions Inventory on an annual basis. The annual emission rates of CH_4 extracted from the inventory were downscaled to hourly emissions rates for comparison with our measurements with an assumption of equal seasonal and diurnal profiles 365 days a year, 24 hours per day; for consistency with upscaling

15 factors used to generate annual emissions (see Figure 8).   While this may be questioned, it should be noted that fugitive emissions of CH_4 from mine faces and tailings ponds in the inventories are estimated based upon emission factors measured at oil sands facilities during summer months (June- Sept), which are then up scaled from hourly emissions to annual emissions using the same assumption that we used to downscale (365 x24), as per recommendation by the Government of Alberta (GOA, 2014).

20 Specifically it is noted from the GOA report that emissions of gaseous species such as CH_4 (and CO_2) are not temperature dependent, (unlike VOC's that have temperature dependent vapour pressures (Li et al., 2017)). The argument used to justify the use of a constant seasonal temporal factor in the GOA report is that temperatures at depth in a tailings pond are said to remain relatively constant throughout the year and thus, biogenic gas formation continues in the winter (GOA, 2014). For mine faces, the

25 GHG component of the oil sand does not change with temperature and is likely released completely in a short period of time after being mined. Thus the government recommendation to oil sand facilities in preparing annual emission estimates of fugitive GHG's is that reduction factors should not to be used in extrapolating summertime emissions over the rest of the year (GOA, 2014). Figure 8 shows a

comparison of the total measured emission rates of CH_4 from the five industrial facilities (2013), the total measured CH_4 emission rate in the AOSR from the single downwind screen on Aug 16, 2013 and the sum of the facility emission rates from the Canadian GHGRP Emissions Inventory for 2013, expressed in hourly units. The combined facility emissions rate of 19.6 ± 1.1 tonnes hr^{-1} is

5 approximately 48 ± 8 % higher than the 5-facility total of 13.2 tonnes hr^{-1} extracted from the inventory for 2013. Facility-to-facility comparisons show higher measured than reported emission rates for three out of the four facilities (SML and SAU facilities are combined as one in the inventory). In contrast, for CNRL our measured emission rate is 1.2 tonnes hr^{-1} lower than the inventory. Since we have determined the composition of SML, SUN and SAJ emissions to be primarily from tailings ponds and

10 open pit mining, there appears to be underestimation in the inventory of those particular area sources within these sites.

These discrepancies indicate a need for inventory reconciliation between the bottom up and top-down estimates. It has been shown possible to reconcile divergent bottom-up and top-down CH_4 estimates for the Barnett Shale by using more comprehensive activity factors and better characterization of emissions

15 from high emitter sites (Lyon et al., 2015) and continuous monitoring to identify these super emitters (Zavala-Araiza et al., 2015). Currently, bottom-up estimates in the AOSR are accomplished by systematic surface flux chamber measurements of area sources (surface mines, tailings ponds) to derive area-based emissions factors (GOA, 2014). While surface flux chamber measurements (Klenbusch, 1986;Conen and Smith, 1998) are estimated to be 50-124% of the true emissions rate for a homogenous

20 source (Klenbusch, 1986), it is unclear how the uncertainty propagates when the emissions factors are scaled to the full surface area of the heterogeneous AOSR emissions sources. The official survey protocol for open pit sources attempts to minimize the possibility of underestimating emissions by explicitly requiring fugitive surveys to include sampling at a range of locations within the open pit mine, where safe to do so, including high priority zones (disturbed in the last week), normal priority

25 zones (disturbed from 1 week to 6 months ago) and low priority zones (disturbed > 6 months ago) (GOA, 2014). However, it seems that the recent core sampling methodology outlined by Johnson et al. (2016) has great promise and reduced uncertainty for estimating fugitive emissions from open pit mining.

Conclusions

We present a detailed approach to identifying and quantifying CH_4 emission sources from the surface mining facilities in the Athabasca Oil Sands Region of Alberta in the year 2013. Emissions of CH_4 are attributed to three major fugitive source types: tailings ponds, open pit mining activity, and emissions from plant facilities. Our method demonstrates the use of BTEX/VOCs as tracers for tailings ponds CH_4 plumes due to the use of diluent, and NO_y/rBC as tracers for surface mining due to heavy hauler diesel trucks operating co-spatially at mine faces in the open pit mines. The combination of SO_2/NO_y is used as a tracer for stack facility plumes which are observed to contain minor but detectable quantities of CH_4, although infrequently. We use the chemical signatures of sources and the screen mass-balance approach for 7 flights to determine total emissions rates of 8.8 ± 0.9 tonnes hr^{-1} from tailings ponds, 45% of total CH_4 emissions in AOSR, 9.8 ± 0.9 tonnes hr^{-1} from open pit surface mining (50%), and 1.0 ± 0.3 tonnes hr^{-1} primary facility-associated and other sources (5%). Open pit mining emissions are measured from all five facilities in the range of 1.2-2.8 tonnes hr^{-1}. In contrast amongst the 19 tailings ponds in the region, CH_4 emissions above determinable levels were only measured from two facilities, SML and SUN. These emissions are likely due to two tailings ponds, MLSB (5.8 ± 0.8 tonnes hr^{-1}) and Ponds 2/3 (2.0 ± 0.3), which are ranked amongst the highest area sources of CH_4 in the region. These results demonstrate the large contributions (~45%) of a few tailings ponds sources to total fugitive CH_4 emissions in the AOSR and highlight opportunities for strategic GHG mitigation. Our individual-plume sum is consistent with estimates derived using the TERRA box approach to determine total emissions within facility boundaries. The agreement between these two methods demonstrates that the three source types listed are representative of the major emissions of CH_4 in the AOSR. Further results from a ~75km flight screen that captured almost all AOSR emissions are able to reproduce total emissions derived from the sum of the five major facilities. Our final top-down estimate of the 2013 summer time emission rate in the region is 19.6 ± 1.1 tonnes CH_4 hr^{-1} or 0.17 ± 0.1 Tg CH_4 yr^{-1}. We note that the annual emissions rate is only a first order approximation of what annual emissions might be if the temporal emissions are constant throughout the year; however, we consider this assumption to be highly uncertain as the seasonality of fugitive emissions rates of CH_4 in the Athabaska Oil Sands region is still a major uncertainty. Further effort should be devoted to measurements of these emission rates in

different seasons, and to understand if ambient temperature and ice coverage on tailings ponds are important parameters or not. Our limited measurements of ethane and methane downwind of the AOSR facilities suggest that the EMR's are quite low, < 1.4%, likely because the fundamental source of the majority of the methane emissions are methanogenic, not thermogenic, in nature. Thus global estimates of the relative contributions of oil and gas emissions to increases in atmospheric CH_4 based on EMR measurements in the free troposphere would not capture AOSR emissions due to the low C_2H_6 emissions in the region.

References

Allen, D., Pickering, K., and Fox-Rabinovitz, M.: Evaluation of pollutant outflow and CO sources during TRACE-P using model-calculated, aircraft-based, and Measurements of Pollution in the Troposphere (MOPITT)-derived CO concentrations, Journal of Geophysical Research: Atmospheres, 109, n/a-n/a, 10.1029/2003JD004250, 2004.

Brandt, A. R., Heath, G. A., Kort, E. A., O'Sullivan, F., Pétron, G., Jordaan, S. M., Tans, P., Wilcox, J., Gopstein, A. M., Arent, D., Wofsy, S., Brown, N. J., Bradley, R., Stucky, G. D., Eardley, D., and Harriss, R.: Methane Leaks from North American Natural Gas Systems, Science, 343, 733-735, 10.1126/science.1247045, 2014.

Bruhwiler, L. M., Basu, S., Bergamaschi, P., Bousquet, P., Dlugokencky, E., Houweling, S., Ishizawa, M., Kim, H. S., Locatelli, R., Maksyutov, S., Montzka, S., Pandey, S., Patra, P. K., Petron, G., Saunois, M., Sweeney, C., Schwietzke, S., Tans, P., and Weatherhead, E. C.: U.S. CH4 emissions from oil and gas production: Have recent large increases been detected?, Journal of Geophysical Research: Atmospheres, 122, 4070-4083, 10.1002/2016JD026157, 2017.

Cambaliza, M. O. L., Shepson, P. B., Caulton, D. R., Stirm, B., Samarov, D., Gurney, K. R., Turnbull, J., Davis, K. J., Possolo, A., Karion, A., Sweeney, C., Moser, B., Hendricks, A., Lauvaux, T., Mays, K., Whetstone, J., Huang, J., Razlivanov, I., Miles, N. L., and Richardson, S. J.: Assessment of uncertainties of an aircraft-based mass balance approach for quantifying urban greenhouse gas emissions, Atmos. Chem. Phys., 14, 9029-9050, 10.5194/acp-14-9029-2014, 2014.

Conen, F., and Smith, K. A.: A re-examination of closed flux chamber methods for the measurement of trace gas emissions from soils to the atmosphere, European Journal of Soil Science, 49, 701-707, 1998.

ECCC: National Inventory Report 1990-2014: Greenhouse Gas Sources and Sinks in Canada, Executive Summary, Environment and Climate Change Canada, Gatineau, QC, 1-14, 2016.

Greenhouse Gas Emissions Reporting Program: Expansion of the GHGRP https://www.ec.gc.ca/ges-ghg/default.asp?lang=En&n=F891687A-1, access: July 27, 2017, 2017a.

Facility Greenhouse Gas Reporting, Greenhouse Gas Emissions Reporting Program: https://www.ec.gc.ca/ges-ghg/default.asp?lang=En&n=040E378D-1, access: July 27, 2017, 2017b.

Edwards, P. M., Young, C. J., Aikin, K., deGouw, J., Dube, W. P., Geiger, F., Gilman, J., Helmig, D., Holloway, J. S., Kercher, J., Lerner, B., Martin, R., McLaren, R., Parrish, D. D., Peischl, J., Roberts, J. M., Ryerson, T. B., Thornton, J., Warneke, C., Williams, E. J., and Brown, S. S.: Ozone photochemistry in an oil and natural gas extraction region during winter: simulations of a snow-free season in the Uintah Basin, Utah, Atmospheric Chemistry and Physics, 13, 8955-8971, 10.5194/acp-13-8955-2013, 2013.

Edwards, P. M., Brown, S. S., Roberts, J. M., Ahmadov, R., Banta, R. M., deGouw, J. A., Dube, W. P., Field, R. A., Flynn, J. H., Gilman, J. B., Graus, M., Helmig, D., Koss, A., Langford, A. O., Lefer, B. L., Lerner, B. M., Li, R., Li, S.-M., McKeen, S. A., Murphy, S. M., Parrish, D. D., Senff, C. J., Soltis, J., Stutz, J., Sweeney, C., Thompson, C. R., Trainer, M. K., Tsai, C., Veres, P. R., Washenfelder, R. A., Warneke, C., Wild, R. J., Young, C. J., Yuan, B., and Zamora, R.: High winter ozone pollution from carbonyl photolysis in an oil and gas basin, Nature, 514, 351-354, 10.1038/nature13767, 2014.

Fujita, E. M., Croes, B. E., Bennett, C. L., Lawson, D. R., Lurmann, F. W., and Main, H. H.: Comparison of Emission Inventory and Ambient Concentration Ratios of CO, NMOG, and NOx in California's South Coast Air Basin, Journal of the Air & Waste Management Association, 42, 264-276, 10.1080/10473289.1992.10466989, 1992.

Fujita, E. M., Watson, J. G., Chow, J. C., and Magliano, K. L.: Receptor model and emissions inventory source apportionments of nonmethane organic gases in California's San Joaquin valley and San Francisco bay area, Atmospheric Environment, 29, 3019-3035, 1995.

Gatti, L. V., Gloor, M., Miller, J. B., Doughty, C. E., Malhi, Y., Domingues, L. G., Basso, L. S., Martinewski, A., Correia, C. S. C., Borges, V. F., Freitas, S., Braz, R., Anderson, L. O., Rocha, H., Grace, J., Phillips, O. L., and Lloyd, J.: Drought sensitivity of Amazonian carbon balance revealed by atmospheric measurements, Nature, 506, 76-80, 10.1038/nature12957, 2014.

GOA: Quantification of area fugitive emissions at oil sands mines, Government of Alberta, AlbertaESRD, Climate Change, 2014, No. 1, 1-15, 2014.

Gordon, M., Li, S. M., Staebler, R., Darlington, A., Hayden, K., O'Brien, J., and Wolde, M.: Determining air pollutant emission rates based on mass balance using airborne measurement data over the Alberta oil sands operations, Atmos. Meas. Tech., 8, 3745-3765, 10.5194/amt-8-3745-2015, 2015.

Hausmann, P., Sussmann, R., and Smale, D.: Contribution of oil and natural gas production to renewed increase in atmospheric methane (2007–2014): top–down estimate from ethane and methane column observations, Atmos. Chem. Phys., 16, 3227-3244, 10.5194/acp-16-3227-2016, 2016.

Helmig, D., Rossabi, S., Hueber, J., Tans, P., Montzka, S. A., Masarie, K., Thoning, K., Plass-Duelmer, C., Claude, A., Carpenter, L. J., Lewis, A. C., Punjabi, S., Reimann, S., Vollmer, M. K., Steinbrecher, R., Hannigan, J. W., Emmons, L. K., Mahieu, E., Franco, B., Smale, D., and Pozzer, A.: Reversal of global atmospheric ethane and propane trends largely due to US oil and natural gas production, Nature Geosci, 9, 490-495, 10.1038/ngeo2721, 2016.

Hendrick, M. F., Ackley, R., Sanaie-Movahed, B., Tang, X., and Phillips, N. G.: Fugitive methane emissions from leak-prone natural gas distribution infrastructure in urban environments, Environmental Pollution, 213, 710-716, 2016.

IPCC: Climate Change 2013: The Physical Science Basis. Contribution of Working Group I to the Fifth Assessment Report of the Intergovernmental Panel on Climate Change, Cambridge University Press, Cambridge, United Kingdom and New York, NY, USA, 1535 pp., 2013.

Jacob, D. J., Turner, A. J., Maasakkers, J. D., Sheng, J., Sun, K., Liu, X., Chance, K., Aben, I., McKeever, J., and Frankenberg, C.: Satellite observations of atmospheric methane and their value for quantifying methane emissions, Atmos. Chem. Phys., 16, 14371-14396, 10.5194/acp-16-14371-2016, 2016.

Jiang, W., Singleton, D. L., Hedley, M., McLaren, R., Dann, T., and Wang, D.: Comparison of Organic Compound Compositions in the Emissions Inventory and Ambient Data for the Lower Fraser Valley, Journal of the Air & Waste Management Association, 47, 851-860, 10.1080/10473289.1997.10464457, 1997.

Johnson, M. R., Crosland, B. M., McEwen, J. D., Hager, D. B., Armitage, J. R., Karimi-Golpayegani, M., and Picard, D. J.: Estimating fugitive methane emissions from oil sands mining using extractive core samples, Atmospheric Environment, 144, 111-123, 2016.

JOSM: Joint Canada/Alberta Implementation Plan for Oil Sands MonitoringISBN: 978-1-100-21630-0, 1-26, 2012.

Karion, A., Sweeney, C., Pétron, G., Frost, G., Michael Hardesty, R., Kofler, J., Miller, B. R., Newberger, T., Wolter, S., Banta, R., Brewer, A., Dlugokencky, E., Lang, P., Montzka, S. A., Schnell, R., Tans, P., Trainer, M., Zamora, R., and Conley, S.: Methane emissions estimate from airborne measurements over a western United States natural gas field, Geophysical Research Letters, 40, 4393-4397, 10.1002/grl.50811, 2013.

Karion, A., Sweeney, C., Kort, E. A., Shepson, P. B., Brewer, A., Cambaliza, M., Conley, S. A., Davis, K., Deng, A., Hardesty, M., Herndon, S. C., Lauvaux, T., Lavoie, T., Lyon, D., Newberger, T., Pétron, G., Rella, C., Smith, M., Wolter, S.,

Yacovitch, T. I., and Tans, P.: Aircraft-Based Estimate of Total Methane Emissions from the Barnett Shale Region, Environmental Science & Technology, 49, 8124-8131, 10.1021/acs.est.5b00217, 2015.

Klenbusch, M. R.: Measurement of gaseous emission rates from land surfaces using an emission isolation chamber, Radian CorporationEPA/600/8-86/008, 58 pages, 1986.

Kort, E. A., Frankenberg, C., Costigan, K. R., Lindenmaier, R., Dubey, M. K., and Wunch, D.: Four corners: The largest US methane anomaly viewed from space, Geophysical Research Letters, 41, 6898-6903, 10.1002/2014GL061503, 2014.

Lavoie, T. N., Shepson, P. B., Cambaliza, M. O. L., Stirm, B. H., Karion, A., Sweeney, C., Yacovitch, T. I., Herndon, S. C., Lan, X., and Lyon, D.: Aircraft-Based Measurements of Point Source Methane Emissions in the Barnett Shale Basin, Environmental Science & Technology, 49, 7904-7913, 10.1021/acs.est.5b00410, 2015.

Li, S.-M., Leithead, A., Moussa, S. G., Liggio, J., Moran, M. D., Wang, D., Hayden, K., Darlington, A., Gordon, M., Staebler, R., Makar, P. A., Stroud, C. A., McLaren, R., Liu, P. S. K., O'Brien, J., Mittermeier, R. L., Zhang, J., Marson, G., Cober, S. G., Wolde, M., and Wentzell, J. J. B.: Differences between measured and reported volatile organic compound emissions from oil sands facilities in Alberta, Canada, Proceedings of the National Academy of Sciences, 10.1073/pnas.1617862114, 2017.

Liggio, J., Li, S.-M., Hayden, K., Taha, Y. M., Stroud, C., Darlington, A., Drollette, B. D., Gordon, M., Lee, P., Liu, P., Leithead, A., Moussa, S. G., Wang, D., O'Brien, J., Mittermeier, R. L., Brook, J. R., Lu, G., Staebler, R. M., Han, Y., Tokarek, T. W., Osthoff, H. D., Makar, P. A., Zhang, J., L. Plata, D., and Gentner, D. R.: Oil sands operations as a large source of secondary organic aerosols, Nature, 534, 91-94, 10.1038/nature17646, 2016.

Lyon, D. R., Zavala-Araiza, D., Alvarez, R. A., Harriss, R., Palacios, V., Lan, X., Talbot, R., Lavoie, T., Shepson, P., Yacovitch, T. I., Herndon, S. C., Marchese, A. J., Zimmerle, D., Robinson, A. L., and Hamburg, S. P.: Constructing a Spatially Resolved Methane Emission Inventory for the Barnett Shale Region, Environmental Science & Technology, 49, 8147-8157, 10.1021/es506359c, 2015.

Mays, K. L., Shepson, P. B., Stirm, B. H., Karion, A., Sweeney, C., and Gurney, K. R.: Aircraft-Based Measurements of the Carbon Footprint of Indianapolis, Environmental Science & Technology, 43, 7816-7823, 10.1021/es901326b, 2009.

McLaren, R., Gertler, A. W., Wittorff, D. N., Belzer, W., Dann, T., and Singleton, D. L.: Real-World Measurements of Exhaust and Evaporative Emissions in the Cassiar Tunnel Predicted by Chemical Mass Balance Modeling, Environmental Science & Technology, 30, 3001-3009, 10.1021/es960036k, 1996.

McLinden, C. A., Fioletov, V., Boersma, K. F., Krotkov, N., Sioris, C. E., Veefkind, J. P., and Yang, K.: Air quality over the Canadian oil sands: A first assessment using satellite observations, Geophysical Research Letters, 39, n/a-n/a, 10.1029/2011GL050273, 2012.

McLinden, C. A., Fioletov, V., Boersma, K. F., Kharol, S. K., Krotkov, N., Lamsal, L., Makar, P. A., Martin, R. V., Veefkind, J. P., and Yang, K.: Improved satellite retrievals of NO_2 and SO_2 over the Canadian oil sands and comparisons with surface measurements, Atmos. Chem. Phys., 14, 3637-3656, 10.5194/acp-14-3637-2014, 2014.

Montzka, S. A., Dlugokencky, E. J., and Butler, J. H.: Non-CO2 greenhouse gases and climate change, Nature, 476, 43-50, 2011.

Peischl, J., Ryerson, T. B., Brioude, J., Aikin, K. C., Andrews, A. E., Atlas, E., Blake, D., Daube, B. C., de Gouw, J. A., Dlugokencky, E., Frost, G. J., Gentner, D. R., Gilman, J. B., Goldstein, A. H., Harley, R. A., Holloway, J. S., Kofler, J., Kuster, W. C., Lang, P. M., Novelli, P. C., Santoni, G. W., Trainer, M., Wofsy, S. C., and Parrish, D. D.: Quantifying

sources of methane using light alkanes in the Los Angeles basin, California, Journal of Geophysical Research: Atmospheres, 118, 4974-4990, 10.1002/jgrd.50413, 2013.

Peischl, J., Ryerson, T. B., Aikin, K. C., de Gouw, J. A., Gilman, J. B., Holloway, J. S., Lerner, B. M., Nadkarni, R., Neuman, J. A., Nowak, J. B., Trainer, M., Warneke, C., and Parrish, D. D.: Quantifying atmospheric methane emissions from the Haynesville, Fayetteville, and northeastern Marcellus shale gas production regions, Journal of Geophysical Research: Atmospheres, 120, 2119-2139, 10.1002/2014JD022697, 2015.

Peischl, J., Karion, A., Sweeney, C., Kort, E. A., Smith, M. L., Brandt, A. R., Yeskoo, T., Aikin, K. C., Conley, S. A., Gvakharia, A., Trainer, M., Wolter, S., and Ryerson, T. B.: Quantifying atmospheric methane emissions from oil and natural gas production in the Bakken shale region of North Dakota, Journal of Geophysical Research: Atmospheres, 121, 6101-6111, 10.1002/2015JD024631, 2016.

Pinto, J.: Atmospheric Chemistry: Wyoming winter smog, Nature Geosci, 2, 88-89, 2009.

Scheff, P. A., and Wadden, R. A.: Receptor modeling of volatile organic compounds. 1. Emission inventory and validation, Environmental Science & Technology, 27, 617-625, 10.1021/es00041a005, 1993.

Schneising, O., Burrows, J. P., Dickerson, R. R., Buchwitz, M., Reuter, M., and Bovensmann, H.: Remote sensing of fugitive methane emissions from oil and gas production in North American tight geologic formations, Earth's Future, 2, 548-558, 10.1002/2014EF000265, 2014.

Schnell, R. C., Oltmans, S. J., Neely, R. R., Endres, M. S., Molenar, J. V., and White, A. B.: Rapid photochemical production of ozone at high concentrations in a rural site during winter, Nature Geosci, 2, 120-122, 2009.

Schnell, R. C., Johnson, B. J., Oltmans, S. J., Cullis, P., Sterling, C., Hall, E., Jordan, A., Helmig, D., Petron, G., Ahmadov, R., Wendell, J., Albee, R., Boylan, P., Thompson, C. R., Evans, J., Hueber, J., Curtis, A. J., and Park, J.-H.: Quantifying wintertime boundary layer ozone production from frequent profile measurements in the Uinta Basin, UT, oil and gas region, Journal of Geophysical Research: Atmospheres, n/a-n/a, 10.1002/2016JD025130, 2016.

Shephard, M. W., McLinden, C. A., Cady-Pereira, K. E., Luo, M., Moussa, S. G., Leithead, A., Liggio, J., Staebler, R. M., Akingunola, A., Makar, P., Lehr, P., Zhang, J., Henze, D. K., Millet, D. B., Bash, J. O., Zhu, L., Wells, K. C., Capps, S. L., Chaliyakunnel, S., Gordon, M., Hayden, K., Brook, J. R., Wolde, M., and Li, S. M.: Tropospheric Emission Spectrometer (TES) satellite observations of ammonia, methanol, formic acid, and carbon monoxide over the Canadian oil sands: validation and model evaluation, Atmos. Meas. Tech., 8, 5189-5211, 10.5194/amt-8-5189-2015, 2015.

Siddique, T., Penner, T., Klassen, J., Nesbø, C., and Foght, J. M.: Microbial Communities Involved in Methane Production from Hydrocarbons in Oil Sands Tailings, Environmental Science & Technology, 46, 9802-9810, 10.1021/es302202c, 2012.

Simpson, I. J., Blake, N. J., Barletta, B., Diskin, G. S., Fuelberg, H. E., Gorham, K., Huey, L. G., Meinardi, S., Rowland, F. S., Vay, S. A., Weinheimer, A. J., Yang, M., and Blake, D. R.: Characterization of trace gases measured over Alberta oil sands mining operations: 76 speciated C_2–C_{10} volatile organic compounds (VOCs), CO_2, CH_4, CO, NO, NO_2, NO_y, O_3 and SO_2, Atmos. Chem. Phys., 10, 11931-11954, 10.5194/acp-10-11931-2010, 2010.

Small, C. C., Cho, S., Hashisho, Z., and Ulrich, A. C.: Emissions from oil sands tailings ponds: Review of tailings pond parameters and emission estimates, Journal of Petroleum Science and Engineering, 127, 490-501, 2015.

Smith, M. L., Kort, E. A., Karion, A., Sweeney, C., Herndon, S. C., and Yacovitch, T. I.: Airborne Ethane Observations in the Barnett Shale: Quantification of Ethane Flux and Attribution of Methane Emissions, Environmental Science & Technology, 49, 8158-8166, 10.1021/acs.est.5b00219, 2015.

5   Strausz, O. P. L., Elizabeth M. : The Chemistry of Alberta Oil Sands, Bitumens and Heavy Oils, Alberta Energy Research Institute, 2003.

Stringham, G.: Chapter 2 - Energy Developments in Canada's Oil Sands, in: Developments in Environmental Science, edited by: Kevin, E. P., Alberta Oil Sands Energy, Industry and the Environment, 11, Elsevier, Oxford, UK, 19-34, 2012.

10

Tokarek, T. W. O.-A., C. A.; Huo, J. A.; McLaren, R.; Lee, A. K.; Gerrit, M.; Willis, M.D.; Abbatt, J.P.D.; Mihele, C.; Darlington, A.; Mittermeier, R. L.; Strawbridge, K.; Hayden, K. L.; Olfert, J. S.; Schnitzler, E.; Brownsey, D. K.; Assad, F. V.; Wentworth, G. R.; Tevlin, A.G.; Worthy, D. E. J.; Murphy, J. G.; Liggio, J.; Brook, J. R.; Osthoff, H. D.: Principal component analysis of ground site measurements in the Athabasca oil sands during summer 2013: Sources of IVOCs,

15   Atmospheric Chemistry and Physics, in preparation, 2017.

Turner, A. J., Jacob, D. J., Benmergui, J., Wofsy, S. C., Maasakkers, J. D., Butz, A., Hasekamp, O., and Biraud, S. C.: A large increase in U.S. methane emissions over the past decade inferred from satellite data and surface observations, Geophysical Research Letters, 43, 2218-2224, 10.1002/2016GL067987, 2016.

20

Turner, A. J., Frankenberg, C., Wennberg, P. O., and Jacob, D. J.: Ambiguity in the causes for decadal trends in atmospheric methane and hydroxyl, Proceedings of the National Academy of Sciences, 114, 5367-5372, 10.1073/pnas.1616020114, 2017.

25   Vaghjiani, G. L., and Ravishankara, A.: New measurement of the rate coefficient for the reaction of OH with methane, Nature, 350, 406-409, 1991.

Walter, D., Heue, K. P., Rauthe-Schöch, A., Brenninkmeijer, C. A. M., Lamsal, L. N., Krotkov, N. A., and Platt, U.: Flux calculation using CARIBIC DOAS aircraft measurements: SO2 emission of Norilsk, Journal of Geophysical Research:

30   Atmospheres, 117, n/a-n/a, 10.1029/2011JD017335, 2012.

Williams, A., and Marcotte, D.: Wind Measurements on a Maneuvering Twin-Engine Turboprop Aircraft Accounting for Flow Distortion, Journal of Atmospheric and Oceanic Technology, 17, 795-810, 2000.

35   Worthy, D. E. J., Chan, E., Ishizawa, M., Chan, D., Poss, C., Dlugokencky, E. J., Maksyutov, S., and Levin, I.: Decreasing anthropogenic methane emissions in Europe and Siberia inferred from continuous carbon dioxide and methane observations at Alert, Canada, Journal of Geophysical Research: Atmospheres, 114, n/a-n/a, 10.1029/2008JD011239, 2009.

Wratt, D. S., Gimson, N. R., Brailsford, G. W., Lassey, K. R., Bromley, A. M., and Bell, M. J.: Estimating regional methane

40   emissions from agriculture using aircraft measurements of concentration profiles, Atmospheric Environment, 35, 497-508, 2001.

Zavala-Araiza, D., Lyon, D., Alvarez, R. A., Palacios, V., Harriss, R., Lan, X., Talbot, R., and Hamburg, S. P.: Toward a Functional Definition of Methane Super-Emitters: Application to Natural Gas Production Sites, Environmental Science &

45   Technology, 49, 8167-8174, 10.1021/acs.est.5b00133, 2015.

Table 1: Enhancements of ΔC_2H_6 from canister measurements overlapping with CH_4 plumes across three flights (Aug 14, Aug 16 and Sep 02). Mean enhanced ΔCH_4 is shown over the course of ~20s canister sampling times with ethane-to-methane ratios (EMRs) computed.

5

Scenario	ΔC_2H_6 (ppb)	ΔCH_4 (ppb)	EMR (%)
SML Ponds (Aug 14)	3.2	814	0.40
SML Mines (Aug 14)	2.6	365	0.72
SUN Ponds (Aug 16)	1.2	215	0.56
SUN Mines (Aug 16)	1.1	185	0.59
CNRL (Sep 02)	1.9	137	1.39

Table 2: Comparison of emissions rates (in tonnes CH_4 hr^{-1}) determined from the screen approach (n estimates per facility), the box-approach (n estimates per facility), and the uncertainty weighted average for each method and facility. The 5-facility AOSR total is show in the final column and row.

10

Method	SML (n)	SUN (n)	CNRL (n)	SAJ (n)	SAU (n)	Total AOSR
Screen	9.1±0.9 (3)	4.2±0.4 (2)	3.6±0.8 (2)	1.2±0.2 (2)	1.4±0.2 (2)	
Box	7.7±1.5 (1)	3.9±0.9 (1)	3.6±0.6 (2)	1.4±0.2 (2)	1.7±0.3 (1)	
Average	8.6±0.9 (4)	4.2±0.4 (3)	3.6±0.5 (4)	1.3±0.2 (4)	1.5±0.2 (3)	**19.2 ± 1.1**
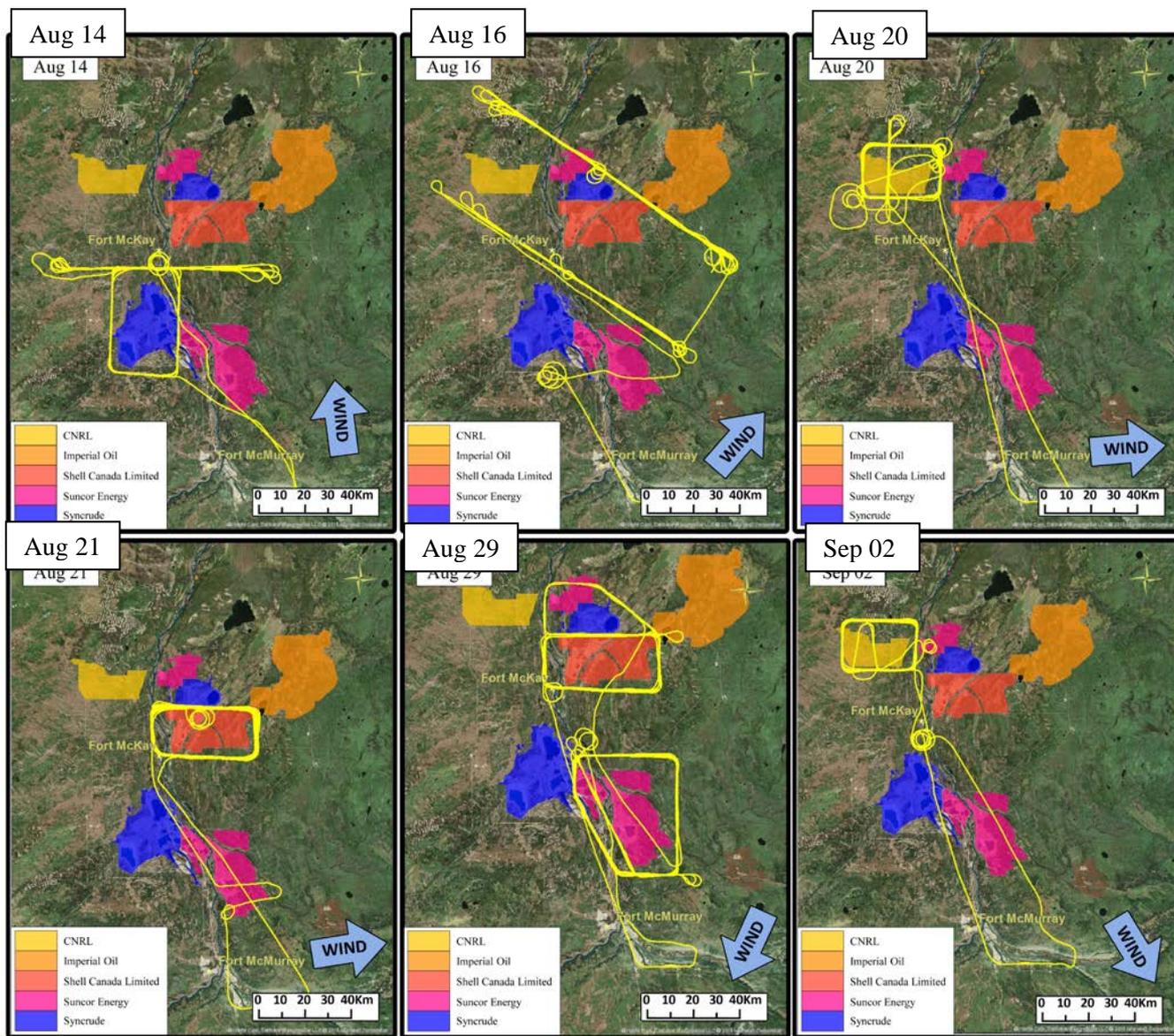
Figure 1: Flight tracks from flights capturing emissions from SML (Aug 14, Aug 16), SUN (Aug 16, Aug 29), CNRL (Aug 20, Sep 02), SAJ (Aug 21, Sep 06 not shown), and SAU (Aug 29, Sep 06 not shown). SML and SAU are shown in blue, SUN in pink, CNRL in yellow and SAJ in dark orange.
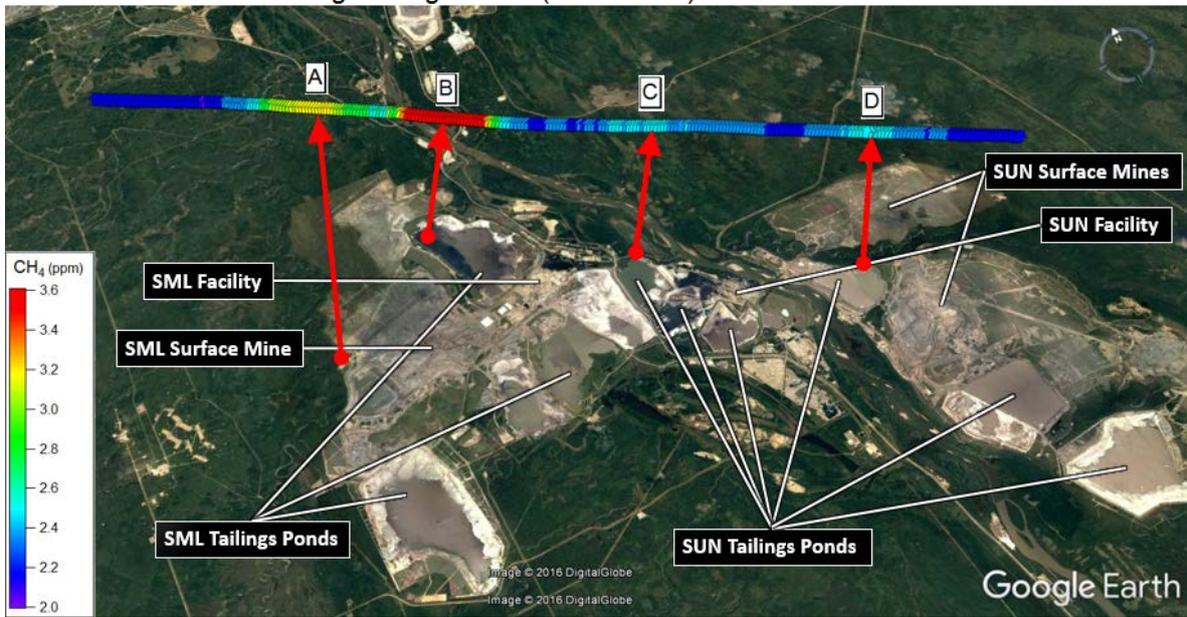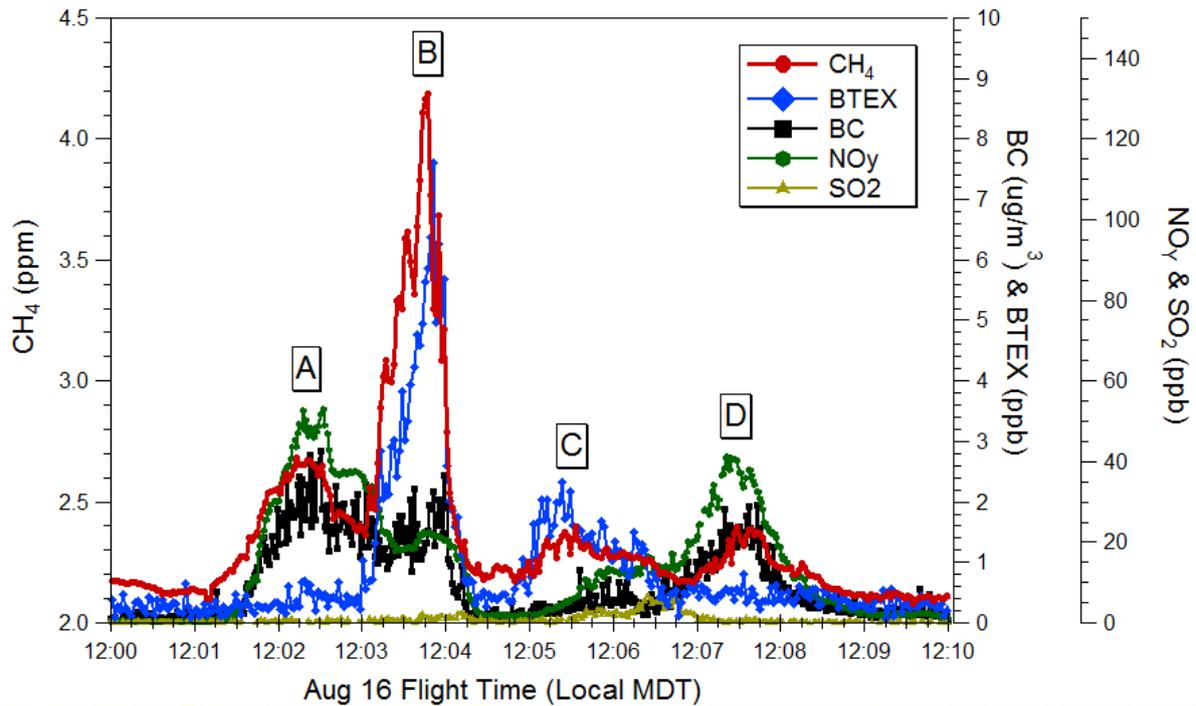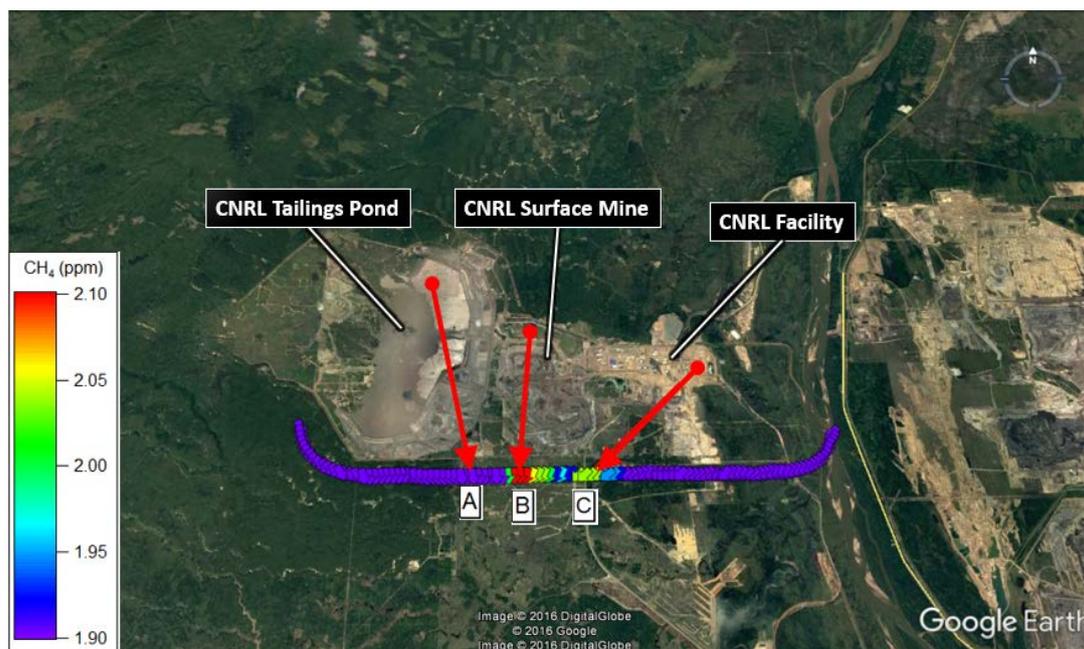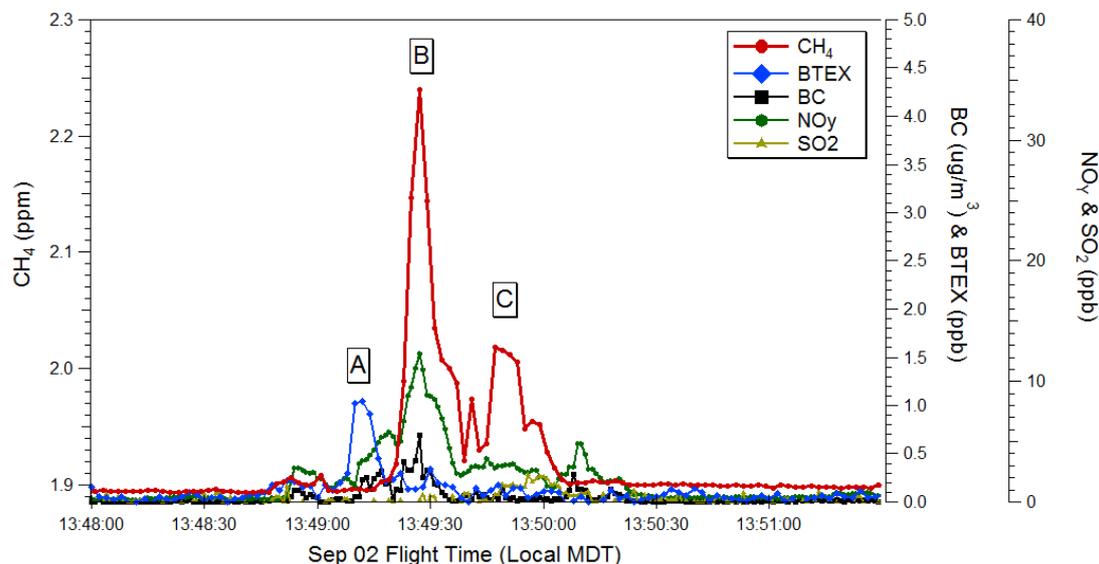
Figure 2: Top: Aircraft measurements of CH4 (red), BTEX (blue) and rBC (black) from a single transect at 150 m agl downwind of SML and SUN on Aug 16. Four plumes are labelled A (SML Mine), B (SML Tailings), C (SUN Tailings), D (SUN Mine). Bottom: CH4 mixing ratios along the 150 m agl transect for the above time series. Each data point is color coded for CH4 mixing ratio as well as instantaneous wind vector measured on the aircraft at that location. Red arrows indicate air parcel back-

trajectories based on linear back extrapolation of the aircraft measured wind vectors at plume centres, with end points at 100 min (A), and 20 min (B-D).

Figure 3: Top: Aircraft measurements of CH$_4$ (red), BTEX (blue) and rBC (black) from single transect ~150 m agl downwind of CNRL. Plume A (CNRL Tailings Pond), Plume B (CNRL Mine) Plume C CNRL Facility. Bottom: CH$_4$ mixing ratios along 150 m agl transect for above time series. Each data point is color coded for CH$_4$ mixing ratio as well as instantaneous wind vector measured on the aircraft

at that location. Red arrows show back-trajectories based on linear extrapolation of measured wind speed and direction.
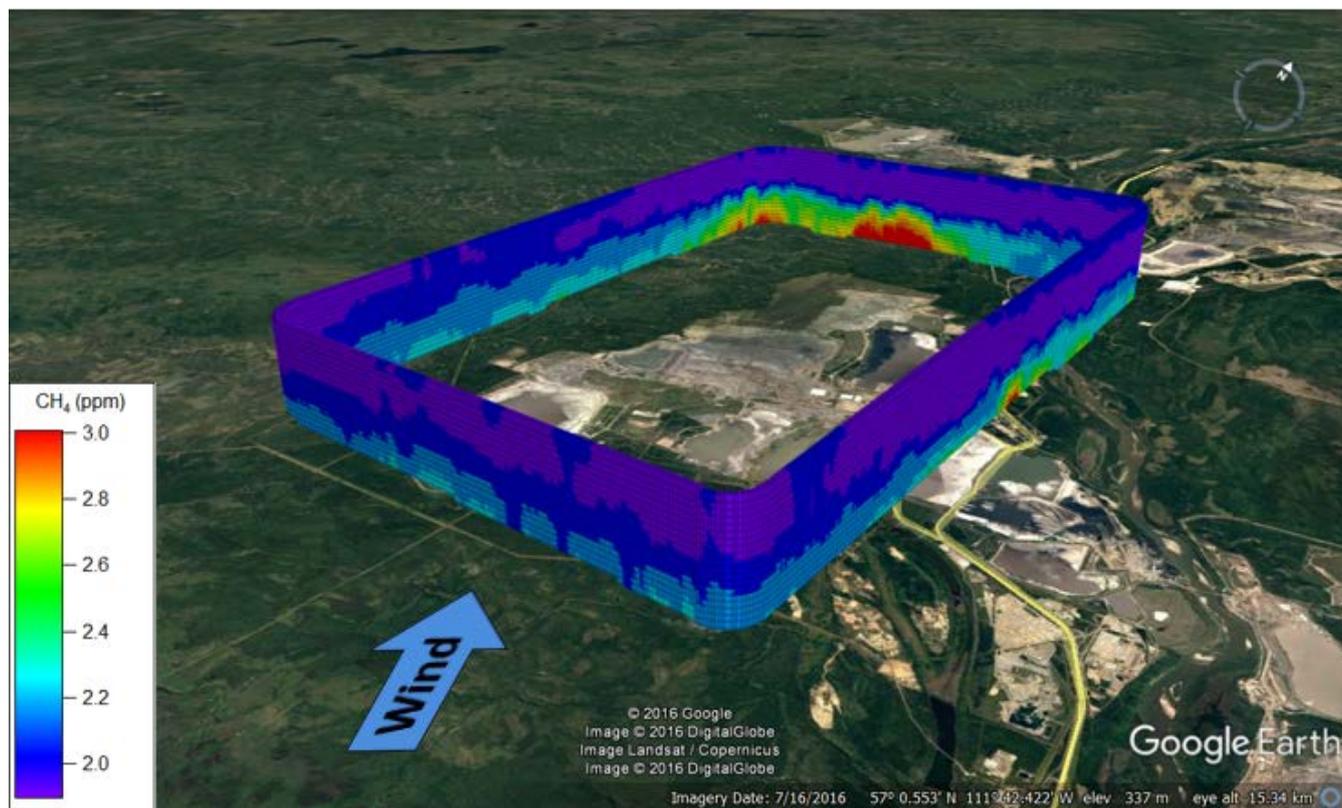
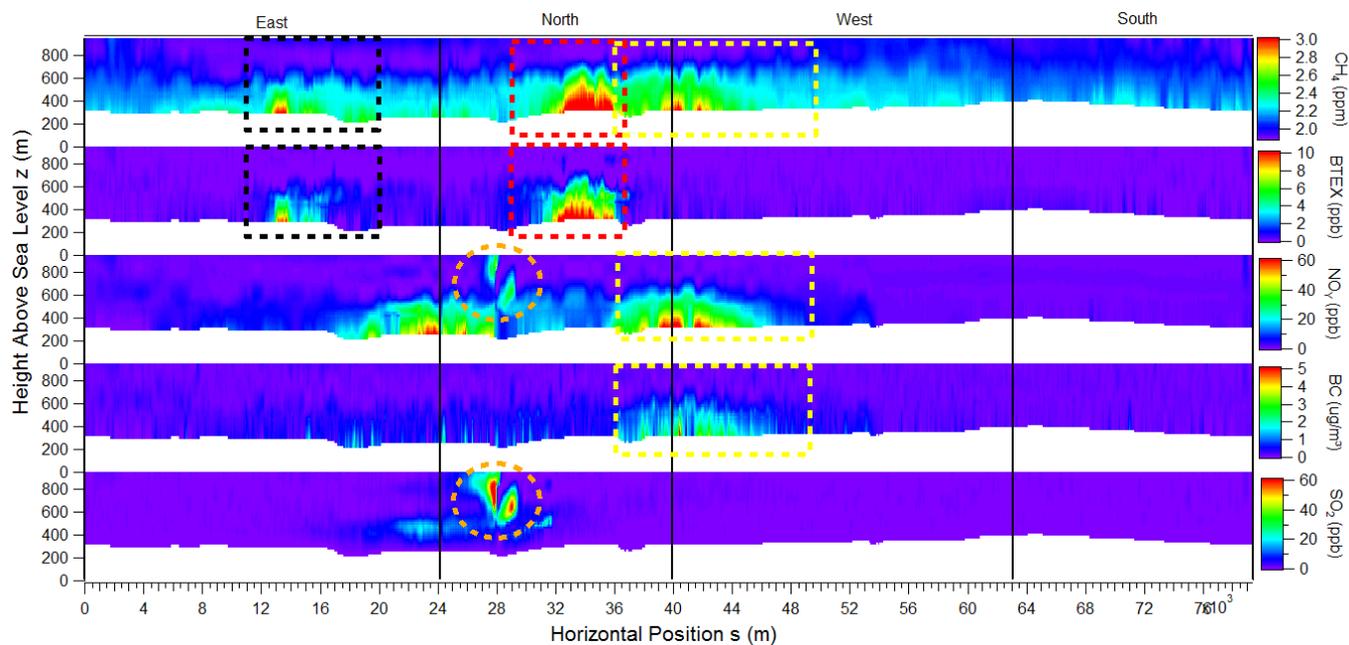5   **Figure 4:** Interpolated CH_4 mixing ratios for the Aug 14 box flight surrounding SML.

10

Figure 5: Curtain plots showing interpolated CH4, BTEX, NOy, rBC and SO2 mixing ratios for the Aug 14 box flight around SML. Red-dashed box indicates the primary plume on the North screen, yellow-dashed box indicates the secondary plume on the West screen, and black-dashed box indicates the tertiary incoming plume on the East screen. Orange dashed-circle shows the upgrader plume on the North screen.
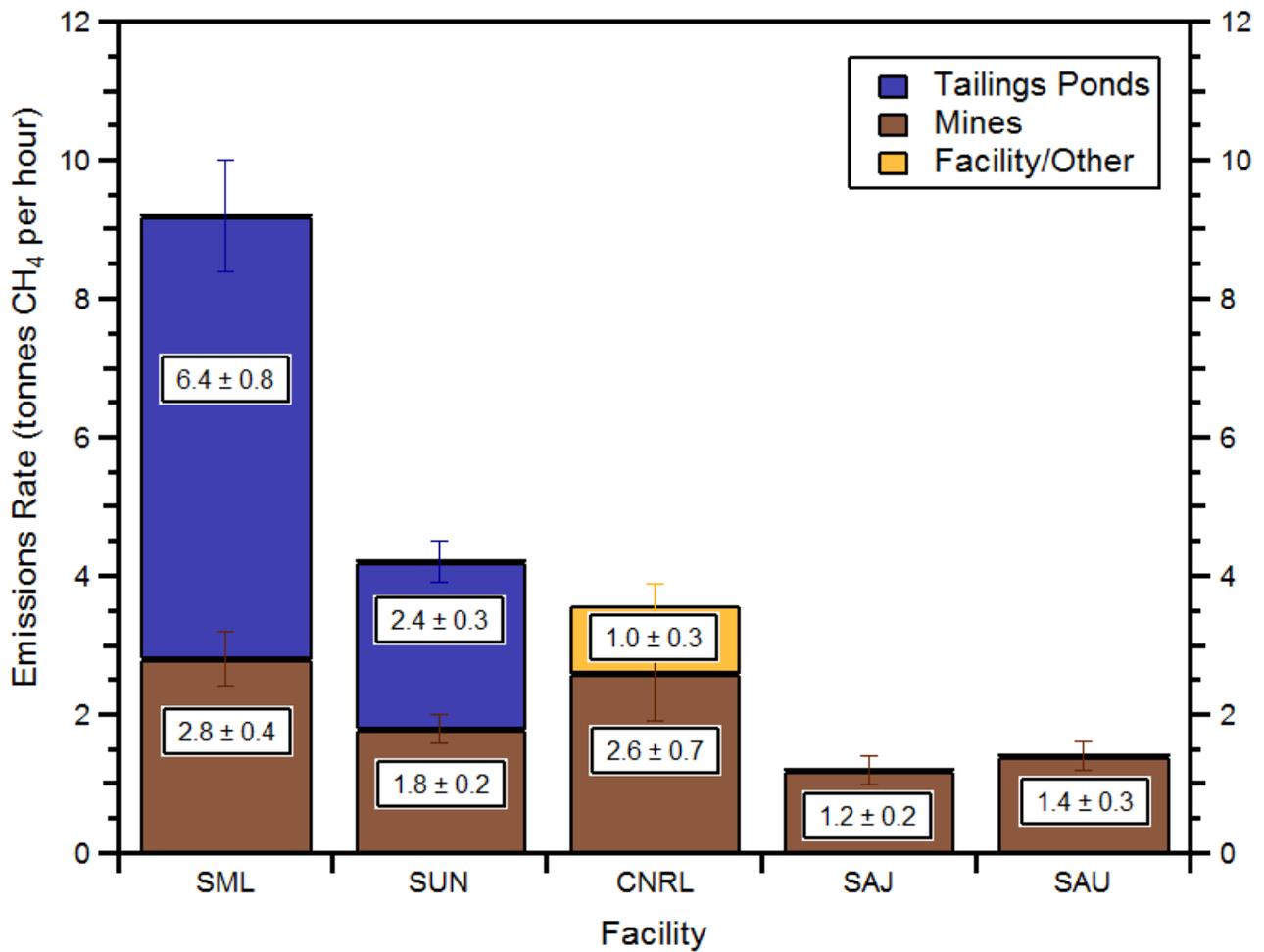
Figure 6: Source-apportioned emissions rates of CH4 determined by the screen mass-balance method (Eq. 1) for the SML, SUN, CNRL, SAJ and SAU facilities. Emissions rates are the average of three mass-balance flights for SML over two days, two flights each for SUN, SAJ and SAU on separate days, and one flight for CNRL.
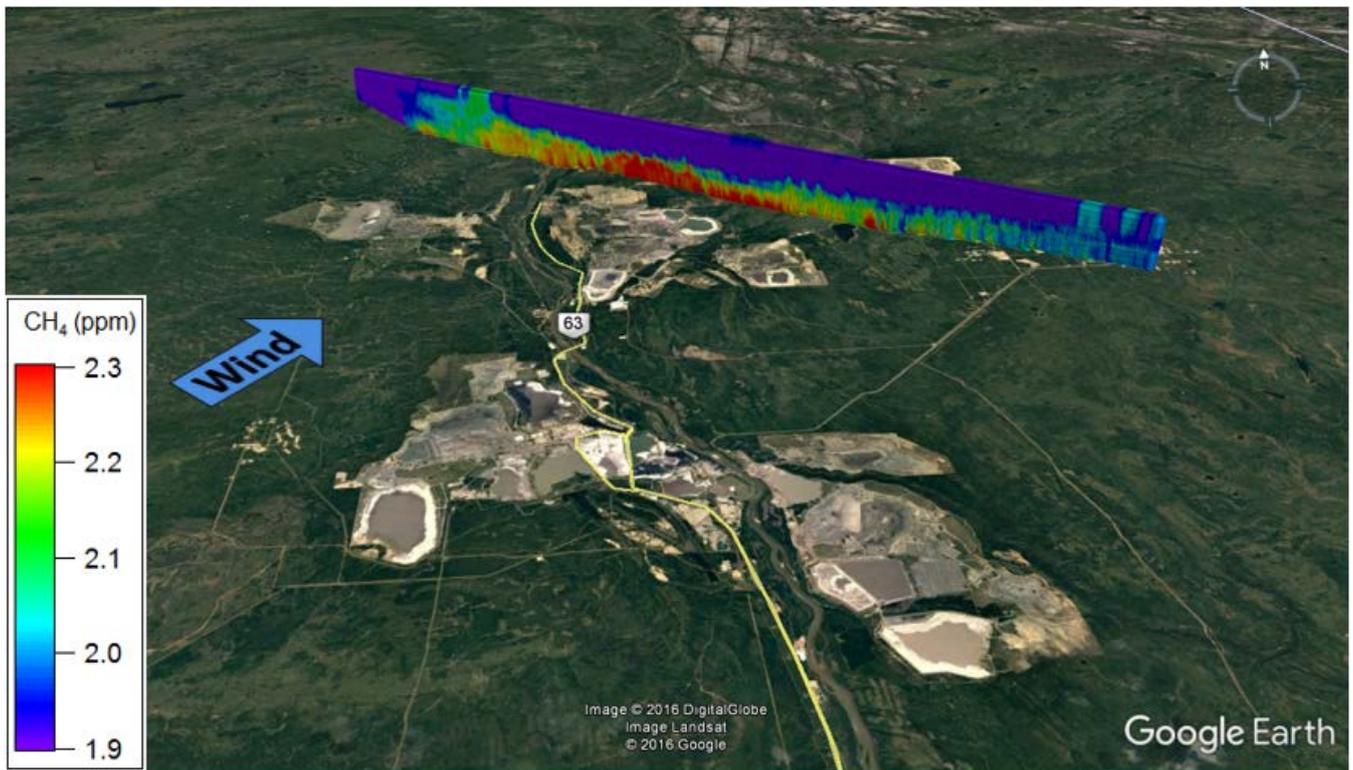
Figure 7: Map image showing interpolated CH$_4$ mixing ratios for the Aug 16 Total Oil Sands screen.
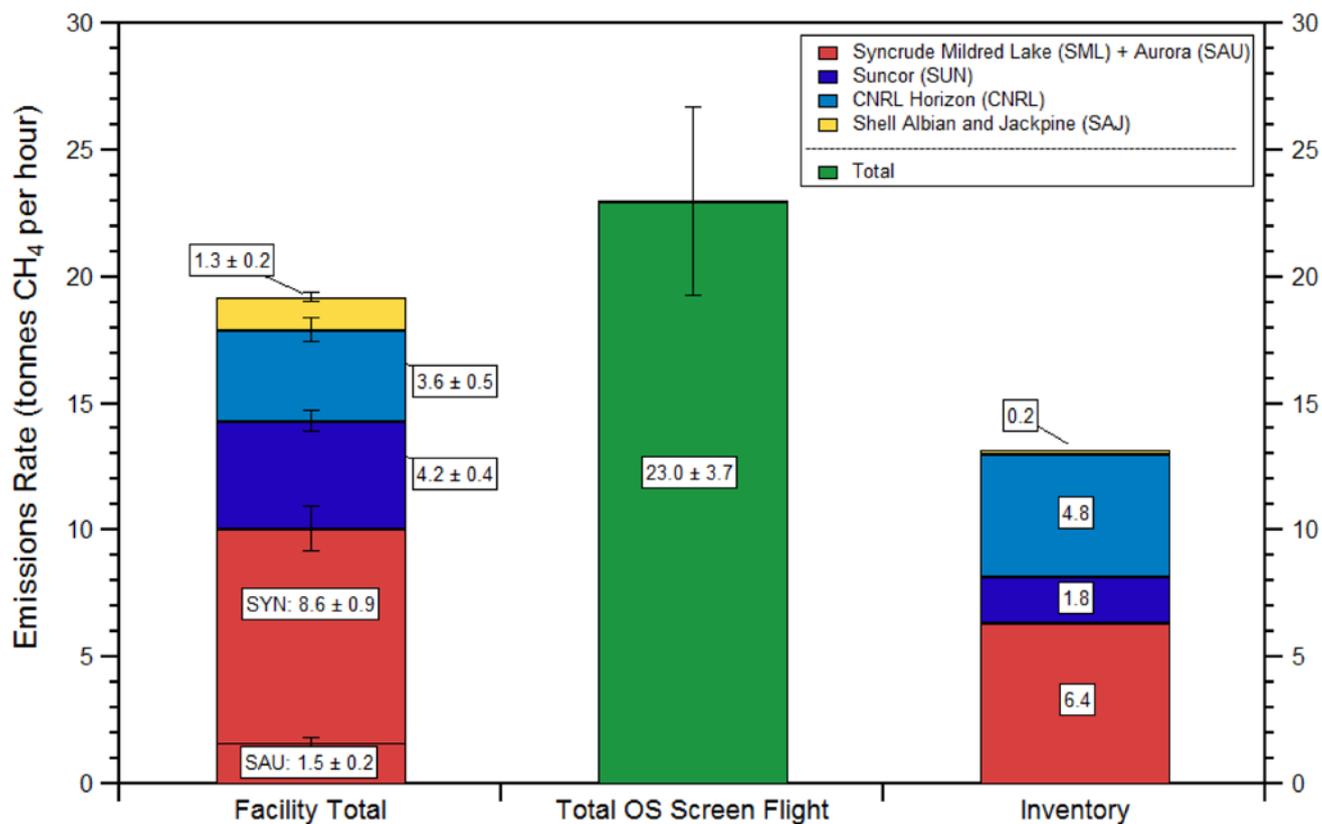
5

Figure 8: Comparison of emissions rates determined for the five major facilities (SML, SAU, SUN, CNRL, SAJ, SAU) with the Total OS Screen Flight (see Fig. 7 for the flight track). Also shown is the CH₄ emissions taken from the Canadian GHGRP Emissions Inventory for the year 2013, scaled down from annual to hourly emissions assuming constant temporal emissions. Note that in the inventory, SML and SAU emissions are reported as a single facility, while our estimates are derived separately.